accumulation ratios and area under the Pt concentration-time curve (AUC) ratios of the tumor to normal tissues at 48 h after injection are summarized in Table 2. The area under the Pt concentration-time curve was calculated based on the trapezoidal rule up to 48 h. As shown in Table 2, the tumor to kidney, liver and spleen ratios were lower than 1 for oxaliplatin, suggesting no selectivity to the tumor. In contrast, the DACHPt/m exhibited accumulation and AUC ratios higher than 1.0, suggesting its selective accumulation in the tumor.

3.2.2. *Effect of P(Glu) block length on the biodistribution of micelles*

The biodistribution of the micelles prepared from PEG-*b*-P(Glu) with different p(Glu) block units in tumor-bearing mice was examined and is shown in Fig. 3. The Pt accumulation levels were studied at 24 and 48 h. All the DACHPt/m formulations showed elevated Pt levels at the tumor (Fig. 3A and B). Importantly, the amount of Pt in liver was directly correlated with the length of the p(Glu) block forming DACHPt/m. The tumor targeting efficiency of the micelles was estimated by calculating the ratio of the accumulated dose in the tumor site against the accumulated dose in the organs (Fig. 3C and D). From these results, DACHPt delivery to the tumor site by a micellar carrier seems to be extremely efficient, since all the micelles showed higher tumor/organ accumulation ratios. This efficiency was maximized for the PEG-*b*-P(Glu) 12–20-micelle formulation showing the lowest non-specific accumulation in normal tissues, thus achieving the highest relative tumor targeting. Such enhanced tumor targeting will permit expanding the therapeutic window of the micelle.

3.3. *Antitumor activity*

To evaluate the antitumor activity of DACHPt/m, CDF1 mice ($n=6$) bearing subcutaneous C-26 cells were treated i.v. four times at 2-day intervals with oxaliplatin at doses of 2, 4, 6, and 10 mg/kg or DACHPt/m (prepared with PEG-*b*-P(Glu) 12–40 and 12–20) at doses of 2, 4, and 6 mg/kg on a Pt basis. Each drug was intravenously injected on days 7, 9, 11, and 13 after inoculation, and the tumor volume after the treatment by oxaliplatin or DACHPt/m with PEG-*b*-P(Glu) 12–40 and 12–20 is shown in Figs. 4 and 5 (A and C), respectively. The relative body weight after the treatment was also monitored and shown in Figs. 4 and 5 (B and D).

The mice treated with 10 mg/kg of oxaliplatin showed toxic death after the fourth injection. Although animals treated with lower oxaliplatin doses did not show significant body weight loss, no inhibition of the tumor growth rate was observed ($p>0.05$). In contrast, the mice treated with 2 mg/kg of DACHPt/m prepared with PEG-*b*-P(Glu) 12–40 achieved significant reduction in the tumor growth rate ($p<0.001$ at day 14) without showing any body weight loss (Fig. 4C and D). Even higher tumor growth inhibition was observed for the mice treated with 4 mg/kg of PEG-*b*-P(Glu) 12–40 DACHPt/m

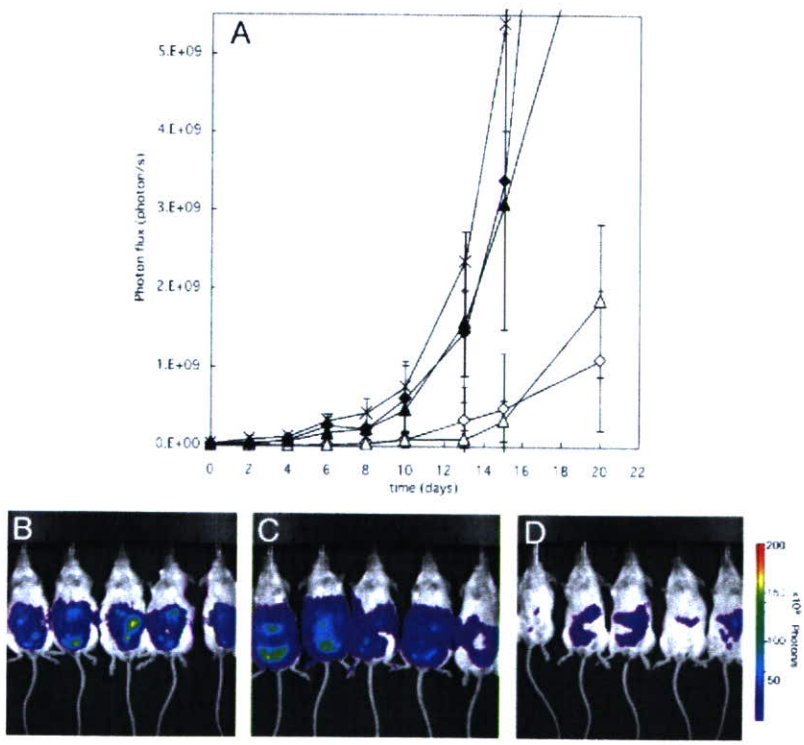

Fig. 6. Antitumor activity of DACHPt-loaded micelle (DACHPt/m) prepared with PEG-*b*-P(Glu) 12–20 against i.p. HeLa-Luc metastases ($n=5$). A. Relative photon flux from intraperitoneal metastatic sites of HeLa-luc *in vivo* treated with oxaliplatin or DACHPt-loaded micelle (DACHPt/m): Saline(×); oxaliplatin at 6 mg/kg(▲); 4 mg/kg(◆); DACHPt/m 12–20 at 6 mg/kg(△); 4 mg/kg(◇). Data are expressed as averages ± S.D. *In vivo* bioluminescent images from HeLa-Luc i.p metastases at day 15: B. Saline; C. oxaliplatin 6 mg/kg; D. DACHPt/m 12–20 at 6 mg/kg.

($p<0.001$ at day 14); however, the 20% body weight loss after fourth injection suggests toxicity intensification. Increasing the DACHPt/m dose to 6 mg/kg resulted in 4 toxic deaths at day 8. The PEG-*b*-P(Glu) 12–20 micelle formulation reduced the toxicity while retaining the antitumor activity of the micelle (Fig. 5C and D). At 2 mg/kg or 4 mg/kg, this micelle formulation showed improved antitumor effect ($p<0.05$ at day 15 for 2 mg/kg; $p<0.01$ at day 15 for 4 mg/kg) compared with oxaliplatin without showing any body weight loss. At 6 mg/kg, the best tumor growth rate reduction was achieved ($p<0.005$ at day 15). The highest dose of this formulation in this experiment did not reach the lethal dose. Thus, PEG-*b*-P(Glu) 12–20 formulation for DACHPt/m seems to radically reduce drug toxicity with maintaining its potent antitumor effect, thus enlarging the therapeutic window. In addition, toxic death with DACHPt/m appeared at lower drug equivalent concentration than with oxaliplatin mainly due to the extremely high plasma AUC of DACHPt/m [22], but also because oxaliplatin is a prodrug of DACHPt. Thus, even though the drug equivalent of DACHPt/m to induce toxic death should be compared with DACHPt, it is very difficult to administer DACHPt alone due to its poor solubility.

Since DACHPt/m prepared with PEG-P(Glu) 12–70 showed higher accumulation to the liver and spleen than DACHPt/m prepared from PEG-P(Glu) 12–20 and 12–40, it will probably not increase the efficiency of the carrier. Therefore, its antitumor activity was not tested.

3.4. Antitumor activity in a bioluminescent intraperitoneal metastasis model

To evaluate the *in vivo* antitumor effect of DACHPt/m on multiple metastases generated from i.p inoculated Hela-Luc cells, SCID mice ($n=5$) were treated with free oxaliplatin or DACHPt/m beginning on day 4 post-injection. Mice with images indicating a successful i.p. inoculation on day 0 and showing *in vivo* evidence of metastasis by day 4 were placed in the drug treatment group. Free oxaliplatin or DACHPt/m were administered i.v a total of three times on day 0, 2, and 4. To quantify the bioluminescent data from metastasis, the photons emitted from the ROI in the whole animal (ventral images) were measured. The mean total photons/s were calculated from all mice. The *in vivo* bioluminescent data indicated that there was a 10-to 50-fold drop in the signal after DACHPt/m treatment (Fig. 6A). Images taken on day 15 (Fig. 6B, C, and D) indicated that DACHPt/m reduced tumor spreading in the peritoneal cavity, showing their strong growth inhibitory effect against the metastatic tumors.

4. Discussion

DACHPt/m were designed to have an extended blood circulation and a selective and high accumulation at the tumor site by the EPR effect. The average diameter of 40 nm and the hydrophilic PEG shell surrounding the micelle core are determinant features of DACHPt/m to avoid the uptake by the RES. Moreover, the sub-100 nm size of micellar nanocarriers might be optimal to achieve a remarkably high tumor extravasation efficiency and deep tumor penetration regardless of the tumor type [26]. The pharmacokinetic parameters of polymeric micelles are significantly modulated by the copolymer architecture. In this regard, the length of the micelle core-forming block not only determines the drug loading capacity of the micelle but also contributes largely to the physicochemical properties of the micelles, whereas PEG length and PEG surface density of micelles have been strongly associated with their long-circulating properties [27,28]. In this study, we prepared DACHPt/m using PEG-*b*-P(Glu) bearing different lengths of p(Glu) chain. We found that this variation considerably influences the biodistribution of micelles and thereby their antitumor activity as well as the final therapeutic window.

Drug dosage in chemotherapy is decided in part based on the competing goals of maximizing the death of malignant cells while minimizing damage to healthy cells. In the case of oxaliplatin, the major and most frequent dose-limiting toxicity observed in clinical trials was neurotoxicity [1]. Toxicological studies performed on rats with cisplatin and oxaliplatin demonstrated that the main target of neurotoxicity was the dorsal root ganglion (DRG) [29]. Although cisplatin accumulated in the DRG at a higher extent than oxaliplatin, the latter displayed more morphometric changes to the DRG after an 8-week recovery period, and this was correlated with a greater retention of oxaliplatin by the DRG in comparison with cisplatin. In contrast, neurotoxic studies revealed that CDDP-loaded micelles did not show any neurotoxicity or neuronal degeneration in rats [21]. This result might be attributed to the marked restriction of platinum accumulation into nervous tissue for the CDDP-loaded micelle, owing to the micelle size and its hydrophilic surface. Since CDDP-loaded micelles and DACHPt/m showed comparable prolonged blood circulation, preferential tumor targeting, and low accumulation in organs (Fig. 2) [20], similar reduction in the platinum accumulation at nervous tissue should be expected for DACHPt/m. Moreover, it has also been suggested that the oxalate group on oxaliplatin might immobilize calcium ions, thereby altering the amplitude of voltage-gated sodium channels of neurons [30]. The absence of an oxalate group in the DACHPt/m formulations eliminates this kind of neuronal damage.

The use of oxaliplatin is also associated with the development of severe sinusoidal injury, an aspect that had not been considered in the earlier clinical trials of oxaliplatin [31,32]. In this regard, the CDDP-loaded micelle prepared with PEG-*b*-P(Glu) 12–40 has shown transient hepatic dysfunction in rats directly related to accumulation of the micelle in liver [21]. In the present study, DACHPt/m prepared with PEG-*b*-P(Glu) 12–40 showed biphasic behavior in liver accumulation, and the Pt level in the liver remarkably increased after 8 h post-injection (Fig. 2B). Thus, the avoidance of liver uptake would be critical for the development of a clinically effective DACHPt/m formulation. We previously reported that the CDDP-loaded micelles also showed rapid accumulation of the micelle in the liver due to the morphological changes of the micelle accompanied by the release of CDDP during circulation [20]. However, such liver accumulation of the CDDP-loaded micelles was reduced for the micelle formulation from PEG-*b*-P(Glu) with a longer PEG segment [20]. Thus, the

coverage of the nanoparticles with PEG palisades is likely to be a crucial factor in the reduced liver accumulation. In this study, we evaluated the effects of the P(Glu) lengths of PEG-*b*-P(Glu) on the accumulation of the micelles in normal tissues and tumors. As a result, the micelles prepared with PEG-*b*-P(Glu) 12–20 showed considerably reduced accumulation in the liver (Fig. 3), resulting in critically reduced toxicity and, in particular, permitted a dosage increase (Fig. 5). Possibly, the use of PEG-*b*-P(Glu) with shorter P (Glu) segments may allow the formation of DACHPt/m with effective surface coverage by PEG probably due to reduced micellar core size, leading to reduction of the liver accumulation of the micelles.

DACHPt/m, prepared with PEG-b-P(Glu) 12–40 or 12–20, presented a remarkable, statistically relevant *in vivo* antitumor activity (Figs. 4 and 5), whereas free oxaliplatin failed to suppress tumor growth. The improved performance of DACHPt/m could be attributed to several aspects. The most distinguishable one is the high and preferential accumulation of DACHPt/m in the tumor due to the prolonged circulation of micelles in the bloodstream as well as the aforementioned EPR effect. In this study, DACHPt/m showed 10 times higher tumor accumulation than free oxaliplatin after 24-h post-injection, and such accumulation was maintained for an extended period (Figs. 2 and 3). On the other hand, free oxaliplatin was rapidly cleared from the bloodstream and the drug level at the tumor site was particularly low (Fig. 2). This accumulation level may be lower than the minimal amount needed to attain an efficient *in vivo* antitumor activity.

The avoidance of permanent drug inactivation by protein binding through the complexation of the platinum to the carboxylic groups in the micelle core could also be responsible for the improved biological performance of DACHPt/m over oxaliplatin. It was previously reported that, immediately after a 1 h infusion of oxaliplatin, approximately 5–30% of the drug is unbound, 10–30% is protein-bound, and 40% form complexes with hemoglobin and small molecular weight compounds in erythrocytes. Three hours later, no oxaliplatin is detectable in the plasma ultrafiltrate and only 10% is detectable in urine [33,34]. Furthermore, as many as 17 biotransformation products of oxaliplatin have been described (conjugation with methionine, cysteine, glutathione, and other low molecular weight species), but only the minor complexes $DACHPtCl_2$, $[DACHPt(H_2O)Cl]^+$ and $[DACHPt(H_2O)_2]^{2+}$ retain the ability to bind to DNA to exert the cytotoxic activity [35,36]. Among them, the dihydroxy product of oxaliplatin has been shown to have significantly greater cellular uptake and cytotoxic properties than its parent compound [37]. However, it represents a very small amount of the total plasma platinum pool after oxaliplatin administration, and therefore might not be a determinant for oxaliplatin cytotoxicity. Moreover, the formation process of $[DACHPt(H_2O)_2]^{2+}$ involves the formation of a reversible intermediate, oxalato monodentate compound, and the dissociation constant for the ring-opening step is below physiological pH (pKa=7.16). This implies that at physiological pH, the reaction favors the deprotonation of the open-ring form and the subsequent formation of the dihydroxy complex, whereas under the acidic conditions of solid tumors, ring-closure is favored and the rapid formation of oxaliplatin would be expected [38]. For DACHPt/m, the biotransformation products might be considerably different from those of oxaliplatin, and probably affect the *in vivo* performance of the drug. Since the discharge of DACHPt products from the micelle core occurs only after cleavage of the polymer-metal complex by chloride ions, and this release is enhanced at low pH, DACHPt/m probably set up conditions that favor the formation of active complexes of oxaliplatin, including the highly active $[DACHPt(H_2O)_2]^{2+}$, leading to an improved efficacy of the drug. Moreover, selective intracellular release of DACHPt complexes might occur after internalization of the micelles by endocytosis in cancer cells. As a result, DACHPt complexes may avoid extracellular inactivation and may readily induced intracellular damage.

Since systemic chemotherapy is not regarded as curative in patients with metastatic tumors and all the established therapies show low efficiency at the late stage of the disease, the antitumor activity of DACHPt/m against an i.p. metastatic tumor model was evaluated to test the potential use of micelles as a therapeutic strategy. Monitoring the development of metastatic disease is currently possible *in vivo* with the use of small animal imaging technologies including bioluminescent imaging. The results demonstrate that free oxaliplatin failed to suppress HeLa-Luc metastatic growth at any dose, whereas DACHPt/m showed a high antitumor activity while controlling tumor dissemination in the peritoneal cavity. This marked difference could be correlated to the extended blood circulation and preferential tumor accumulation of DACHPt/m, although further experiments are necessary to determine the effect of the metastatic disposition on the efficiency of the micelle. The present results revealed that DACHPt/m has a high level of antitumor activity not only on primary solid tumors but also against metastatic tumors, suggesting that DACHPt/m could be an outstanding drug delivery system for metastasis treatment.

In conclusion, we have demonstrated that decreasing the length of the core-forming block of DACHPt/m augmented their tumor specificity and drastically diminished their toxicity. Moreover, the high and preferential accumulation of the micelles at the tumor site resulted in considerable antitumor activity of DACHPt/m against primary and metastatic tumor models. Thus, DACHPt/m might be an exceptional drug delivery system for oxaliplatin active complexes.

Acknowledgments

This research was supported by a Grant-in-Aid for Scientific Research from Ministry of Education, Culture, Sports, Science and Technology of Japan as well as by the Project on the Materials Development for Innovative Nano-Drug Delivery Systems from the Ministry of Education, Culture, Sports, Science and Technology (MEXT), Japan.

References

[1] A. Ibrahim, S. Hirschfeld, M.H. Cohen, D.J. Griebel, G.A. Williams, R. Pazdur, FDA drug approval summaries: oxaliplatin, Oncologist 9 (2004) 8–12.

[2] J.M. Extra, M. Espie, F. Calvo, Phase I study of oxaliplatin in patients with advanced cancer, Cancer Chemother. Pharmacol. 25 (1990) 299–303.

[3] G. Mathé, Y. Kidani, M. Segiguchi, M. Eriguchi, G. Fredj, G. Peytavin, J.L. Misset, S. Brienza, F. de Vassals, E. Chenu, C. Bourut, Oxalato-platinum or l-OHP, a third generation platinum complex: an experimental and clinical appraisal and preliminary comparison with cis-platinum and carboplatinum, Biomed. Pharmacother. 43 (1989) 237–250.
[4] Y. Matsumura, H. Maeda, A new concept for macromolecular therapeutics in cancer chemotherapy: mechanism of tumoritropic accumulation of proteins and the antitumor agent SMANCS, Cancer Res. 46 (1986) 6387–6392.
[5] M. Yatvin, H. Miihlensiepen, W. Porschen, L. Feinendegen, J. Weinstein, Selective delivery of liposome-associated cis-dichloro-diammine platinum (II) by heat and its influence on tumor drug uptake and growth, Cancer Res. 41 (1981) 1602–1607.
[6] R. Perez-Soler, Liposomes as carriers of antitumor agents: toward a clinical reality, Cancer Treatment Rev. 16 (1989) 67–82.
[7] R. Perez-Soler, I. Han, S. Al-Baker, A.R. Khokhar, Lipophilic platinum complexes entrapped in liposomes: improved stability and preserved antitumor activity with complexes containing linear alkyl carboxylate leaving groups, Cancer Chemother. 33 (1994) 378–384.
[8] D. Avichechter, B. Schechter, R. Arnon, Functional polymers in drug delivery: carrier-supported CDDP (cis-platin) complexes carboxylates — effect on human ovarian carcinoma, React. Funct. Polym. 36 (1998) 59–69.
[9] B. Schechner, A. Newman, M. Wilnek, R. Arnon, Soluble polymers as carriers of cis-platinum, J. Control. Release 39 (1989) 75–87.
[10] X. Lin, Q. Zhang, J.R. Rice, D.R. Stewart, D.P. Nowotnik, S.B. Howell, Improved targeting of platinum chemotherapeutics. The antitumour activity of the HPMA copolymer platinum agent AP5280 in murine tumour models, Eur J Cancer. 40 (2004) 291–297.
[11] J.R. Rice, J.L. Gerberich, D. Nowotnik, S.B. Howell, Preclinical efficacy of AP5346, a novel diaminocyclohexane-platinum tumor-targeting drug delivery system, Clin. Cancer Res. 12 (2006) 2248–2254.
[12] K. Kataoka, G.S. Kwon, M. Yokoyama, Y. Sakurai, T. Okano, Block copolymer micelles as vehicles for drug delivery, J. Control. Release 24 (1993) 119–132.
[13] C. Allen, D. Mysinger, A. Eisenberg, Nano-engineering block copolymer aggregates for drug delivery, Colloids Surf., B Biointerfaces 16 (1999) 3–27.
[14] N. Nishiyama, K. Kataoka, Nano-structured devices based on block copolymer assemblies for drug delivery: designing structures for enhanced drug function, Adv. Polym. Sci. 193 (2006) 67–101.
[15] H.M. Aliabadi, A. Lavasanifar, Polymeric micelles for drug delivery, Expert Opin. Drug Deliv. 3 (2006) 139–161.
[16] N. Nishiyama, M. Yokoyama, T. Aoyagi, T. Okano, Y. Sakurai, K. Kataoka, Preparation and characterization of self-assembled polymer-metal complex micelle from cis-dichlorodiammineplatinum(II) and poly(ethylene glycol)-poly(a,b-aspartic acid) block copolymer in an aqueous medium, Langmuir 15 (1999) 377–383.
[17] N. Nishiyama, K. Kataoka, Preparation and characterization of size-controlled polymeric micelle containing cis-dichlorodiammineplatinum(II) in the core, J Control. Release 74 (2001) 83–94.
[18] N. Nishiyama, Y. Kato, Y. Sugiyama, K. Kataoka, Cisplatin-loaded polymer-metal complex micelle with time-modulated decaying property as a novel drug delivery system, Pharm. Res. 18 (2001) 1035–1041.
[19] N. Nishiyama, F. Koizumi, S. Okazaki, Y. Matsumura, K. Nishio, K. Kataoka, Differential gene expression profile between PC-14 cells treated with free cisplatin and cisplatin-incorporated polymeric micelles, Bioconjug. Chem. 14 (2003) 449–457.
[20] N. Nishiyama, S. Okazaki, H. Cabral, M. Miyamoto, Y. Kato, Y. Sugiyama, K. Nishio, Y. Matsumura, K. Kataoka, Novel cisplatin-incorporated polymeric micelles can eradicate solid tumors in mice, Cancer Res. 63 (2003) 8977–8983.
[21] H. Uchino, Y. Matsumura, T. Negishi, F. Koizumi, T. Hayashi, T. Honda, N. Nishiyama, K. Kataoka, S. Naito, T. Kakizoe, Cisplatin-incorporating polymeric micelles (NC-6004) can reduce nephrotoxicity and neurotoxicity of cisplatin in rats, Br. J. Cancer 93 (2005) 678–687.
[22] H. Cabral, N. Nishiyama, S. Okazaki, H. Koyama, K. Kataoka, Preparation and biological properties of dichloro(1,2-diaminocyclohexane)platinum (II) (DACHPt)-loaded polymeric micelles, J. Control. Release 101 (2005) 223–232.
[23] T. Tashiro, Y. Kawada, Y. Sakurai, Y. Kidani, Antitumor activity of a new platinum complex: oxalato (trans-l-diaminocyclohexane) platinum (II): new experimental data, Biomed. Pharmacother. 43 (1989) 251–260.
[24] S. Oppenheimer, Cellular basis of cancer metastasis: a review of fundamentals and new advances, Acta Histochem. 108 (2006) 327–334.
[25] Cervical cancer, NIH Consens. Statement 14 (1996) 1–38.
[26] A. Lukyanov, Z. Gao, L. Mazzola, V.P. Torchilin, Polyethylene glycol-dyacyllipid micelles demonstrate increased accumulation in subcutaneous tumors in mice, Pharm. Res. 19 (2002) 1424–1429.
[27] G.S. Kwon, S. Suwa, M. Yokoyama, T. Okano, Y. Sakurai, K. Kataoka, Enhanced tumor accumulation and prolonged circulation times of micelles-forming poly(ethyleneoxide-aspartate) block copolymers-adriamycin conjugates, J. Control. Release 29 (1994) 17–23.
[28] M. Yokoyama, T. Okano, Y. Sakurai, S. Fukushima, K. Okamoto, K. Kataoka, Selective delivery of adriamycin to a solid tumor using a polymeric micelle carrier system, J. Drug Target. 7 (1999) 171–186.
[29] G. Cavaletti, G. Tredici, M.G. Petruccioli, E. Donde, P. Tredici, P. Marmiroli, C. Minoia, A. Ronchi, M. Bayssas, G. Griffon Etienne, Effects of different schedules of oxaliplatin treatment on the peripheral nervous system of the rat, Eur. J. Cancer 37 (2001) 2457–2463.
[30] F. Grolleau, L. Gamelin, M. Boisdron-Celle, B. Lapied, M. Pelhate, E. Gamelin, A possible explanation for a neurotoxic effect of the anticancer agent oxaliplatin on neuronal voltage-gated sodium channels, J. Neurophysiol. 85 (2001) 2293–2297.
[31] L. Rubbia-Brandt, V. Audard, P. Sartoretti, A.D. Roth, C. Brezault, M. Le Charpentier, B. Dousset, P. Morel, O. Soubrane, S. Chaussade, G. Mentha, B. Terris, Severe hepatic sinusoidal obstruction associated with oxaliplatin based chemotherapy in patients with metastatic colorectal cancer, Ann. Oncol. 15 (2004) 460–466.
[32] G. Tisman, D. MacDonald, N. Shindell, E. Reece, P. Patel, N. Honda, E.K. Nishimora, J. Garris, W. Shannahan, N. Chisti, J. McCarthy, S.N. Moaddeli, D. Sargent, A. Plant, Oxaliplatin toxicity masquerading as recurrent colon cancer, J. Clin. Oncol. 22 (2004) 3202–3204.
[33] J. Liu, E. Kraut, J. Bender, R. Brooks, S. Balcerzak, M. Grever, H. Stanley, S. D'Ambrosio, R. Gibson-D'Ambrosio, K.K. Chan, Pharmacokinetics of oxaliplatin (NSC266046) alone and in combination with paclitaxel in cancer patients, Cancer Chemother. Pharmacol. 49 (2002) 367–374.
[34] C. Massari, S. Brienza, M. Rotarski, J. Gastiaburu, J.-L. Misset, D. Cupissol, E. Alafaci, H. Dutertre-Catella, G. Bastian, Pharmacokinetics of oxaliplatin in patients with normal versus impaired renal function, Cancer Chemother. Pharmacol. 45 (2000) 157–164.
[35] F.R. Luo, S.D. Wyrick, S.G. Chaney, Biotransformations of oxaliplatin in rat blood *in vitro*, J. Biochem. Molec. Toxicol. 13 (1999) 159–169.
[36] F.R. Luo, T.-Y. Yen, S.D. Wyrick, S.G. Chaney, High-performance liquid chromatographic separation of the biotransformation products of oxaliplatin, J. Chromatogr., B 724 (1999) 345–356.
[37] F.R. Luo, S.D. Wyrick, S.G. Chaney, Cytotoxicity, cellular uptake and cellular biotransformations of oxaliplatin in human colon carcinoma cells, Oncol. Res. 10 (1998) 595–603.
[38] E. Jerremalm, P. Videhult, G. Alvelius, W.J. Griffiths, T. Bergman, S. Eksborg, H. Ehrsson, Alkaline hydrolysis of oxaliplatin — isolation and identification of the oxalato monodentate intermediate, J. Pharm. Sci. 91 (2002) 2116–2121.

Cyclic RGD Peptide-Conjugated Polyplex Micelles as a Targetable Gene Delivery System Directed to Cells Possessing $\alpha_v\beta_3$ and $\alpha_v\beta_5$ Integrins

Makoto Oba,[†] Shigeto Fukushima,[‡,§] Naoki Kanayama,[§,¶] Kazuhiro Aoyagi,[§] Nobuhiro Nishiyama,[#] Hiroyuki Koyama,[†] and Kazunori Kataoka*[,§,¶,#,⊥]

Department of Clinical Vascular Regeneration, Graduate School of Medicine, The University of Tokyo, 7-3-1 Hongo, Bunkyo, Tokyo 113-8655, Japan, R&D Division, Pharmaceuticals Group, Nippon Kayaku Co., Ltd., Department of Materials Engineering, Graduate School of Engineering, The University of Tokyo, 7-3-1 Hongo, Bunkyo, Tokyo 113-8656, Japan, CREST, Japan Science and Technology Agency, Japan, Center for Disease Biology and Integrative Medicine, Graduate School of Medicine, The University of Tokyo, 7-3-1 Hongo, Bunkyo, Tokyo 113-0033, Japan, and Center for NanoBio Integration, The University of Tokyo, 7-3-1 Hongo, Bunkyo, Tokyo 113-8656, Japan. Received January 15, 2007; Revised Manuscript Received May 11, 2007

A cyclic RGD peptide-conjugated block copolymer, cyclo[RGDfK(CX-)]−poly(ethylene glycol)−polylysine (c(RGDfK)−PEG−PLys), was synthesized from acetal-PEG−PLys under mild acidic conditions and spontaneously associated with plasmid DNA (pDNA) to form a polyplex micelle in aqueous solution. The cyclic RGD peptide recognizes $\alpha_v\beta_3$ and $\alpha_v\beta_5$ integrin receptors, which play a pivotal role in angiogenesis, vascular intima thickening, and the proliferation of malignant tumors. The c(RGDfK)−PEG−PLys/pDNA polyplex micelle showed a remarkably increased transfection efficiency (TE) compared to the PEG−PLys/pDNA polyplex micelle for the cultured HeLa cells possessing $\alpha_v\beta_3$ and $\alpha_v\beta_5$ integrins. On the other hand, in the transfection against the 293T cells possessing no $\alpha_v\beta_3$ and a few $\alpha_v\beta_5$ integrins, the TE of the c(RGDfK)−PEG−PLys/pDNA micelle showed no increase compared to the TE of the PEG−PLys/pDNA micelle. Flow cytometric analysis revealed a higher uptake of the c(RGDfK)−PEG−PLys/pDNA micelle than the PEG−PLys/pDNA micelle against HeLa cells, consistent with the transfection results. Furthermore, a confocal laser scanning microscopic observation revealed that the pDNA in the c(RGDfK)−PEG−PLys micelle preferentially accumulated in the perinuclear region of the HeLa cells within 3 h of incubation. No such fast and directed accumulation of pDNA to the perinuclear region was observed for the micelles without c(RGDfK) ligands. These results indicate that the increase in the TE induced by the introduction of the c(RGDfK) peptide ligand was due to an increase in cellular uptake as well as facilitated intracellular trafficking of micelles toward the perinuclear region via $\alpha_v\beta_3$ and $\alpha_v\beta_5$ integrin receptor-mediated endocytosis, suggesting that the cyclic RGD peptide-conjugated polyplex micelle has promising feasibility as a site-specifically targetable gene delivery system.

INTRODUCTION

With the increase in available information on various disease genes that has resulted from progress in the Human Genome Project, gene therapy is increasingly recognized as a promising therapy for many intractable diseases. Obviously, a major key to successful gene therapy is the development of gene vectors that are particularly effective for *in vivo* use. Nevertheless, there are many restrictions in the clinical application of viral vectors, which have played a pivotal role in gene therapy up to now, because of their safety issues, including antigenicity, as well as to the difficulty of formulating them with good quality control. These limitations of viral vectors have led to the recent trend in developing nonviral vectors with safety and high productivity as alternative systems to viral vectors.

One of the important challenges in the development of nonviral vectors is the system available for systemic injection, which must be stable enough to achieve longevity in the blood circulation but also be able to achieve high transfection efficiency (TE) in the target region with minimal toxicity. Lipoplex (*1*) and polyplex (*2*) systems based on cationic lipids and polymers, respectively, have been extensively studied as nonviral gene vectors for systemic administration. Nevertheless, there remain unresolved issues with these systems, because it is generally required that they contain excessive cationic lipids or polymers to increase solubility in an aqueous solution. Eventually, shifting their surface charge to a positive value induces nonspecific interaction with anionic components in the body such as plasma proteins and blood cells. This apparently hampers their applicability to systemic gene delivery. Polyplex micelles (*3*), characterized by the unique core−shell architecture of the hydrophilic shell layer surrounding their polyplex core, have the potential to acquire a so-called "stealth" property to minimize nonspecific interaction with biocomponents. Indeed, a polyplex micelle with poly(ethylene glycol) (PEG) as a hydrophilic shell layer achieved high stability in a medium containing serum compared to conventional lipoplexes and polyplexes and showed increased retention time in the bloodstream (*4*, *5*), suggesting that a polyplex micelle may be a promising candidate for a vector that can be used in systemic gene delivery. Nevertheless, in order to increase selective uptake into the target cells, appropriate ligands are preferably introduced into the surface of the polyplex micelles. In this way, surface-installed ligands are expected to enhance the uptake rate of the

* To whom correspondence should be addressed. Tel: +81-3-5841-7138, fax: +81-3-5841-7139, e-mail: kataoka@bmw.t.u-tokyo.ac.jp.
† Department of Clinical Vascular Regeneration, The University of Tokyo.
‡ Nippon Kayaku Co., Ltd.
§ Department of Materials Engineering, The University of Tokyo.
¶ CREST.
# Graduate School of Medicine, The University of Tokyo.
⊥ Center for NanoBio Integration, The University of Tokyo.

10.1021/bc0700133 CCC: $37.00
Published on Web 06/27/2007

polyplex micelles into the target cells by receptor-mediated endocytosis, which may lead to higher gene TE compared to the ligand-free polyplex micelles taken up by the cells through adsorptive or fluid-phase endocytosis (*6*–*8*).

In this study, acetal-poly(ethylene glycol)–polylysine (acetal-PEG–PLys) was synthesized as a precursor for constructing ligand-installed polyplex micelles. PLys, which is one of the first polymers used and well studied as a nonviral vector, was chosen as a cationic segment of the block copolymer. PLys-based polyplexes are known to show a relatively low TE against cultured cell lines compared to those having the endosomal escape function, such as polyethylenimine (PEI)-based polyplexes, but they have an advantage in stability even in a diluted condition, and they have shown an appreciable level of gene transfection in animal models (*5*, *9*). A cyclic RGD peptide (c(RGDfK)), which selectively recognizes $\alpha_v\beta_3$ and $\alpha_v\beta_5$ integrin receptors (*10*), was chosen as a ligand and introduced into the PEG terminus of aldehyde-PEG–PLys, derived from acetal-PEG–PLys, through a thiazolidine ring formation, and the c(RGDfK)–PEG–PLys block copolymer was obtained. It is generally known that the $\alpha_v\beta_3$ and $\alpha_v\beta_5$ integrins are expressed on various cell types such as endothelial cells, osteoclasts, macrophages, platelets, and melanomas, and that they play a significant role in angiogenesis, vascular intima thickening, and the proliferation of malignant tumors (*11*). Therefore, gene delivery targeting the $\alpha_v\beta_3$ and $\alpha_v\beta_5$ integrins is expected to be useful in the treatment of cancer and vascular diseases. Indeed, the c(RGDfK)–PEG–PLys/pDNA polyplex micelle thus prepared showed a remarkably increased TE compared to ligand-free polyplex micelles against the HeLa cells expressing $\alpha_v\beta_3$ and $\alpha_v\beta_5$ integrins.

EXPERIMENTAL PROCEDURES

Materials. 3,3-Diethoxypropanol was purchased from Aldrich Chemical Co. Ltd. (Milwaukee, WI). Ammonia solution (25%), tetrahydrofuran (THF), *N,N*-dimethylformamide (DMF), *n*-hexane, methanesulfonyl chloride (MsCl), and triethylamine (TEA) were purchased from Wako Pure Chem. Co. Ltd. (Japan). Ethylene oxide (EO) was purchased from Sumitomo Seika Chemicals Co. Ltd. (Japan). THF was distilled according to the conventional procedure as previously reported (*12*). DMF was dehydrated using activated molecular sieves (4A) and distilled under reduced pressure. 3,3-Diethoxypropanol and *n*-hexane were distilled over sodium wire. MsCl, TEA, and EO were dried over calcium hydride followed by distillation. CXYGGRGDS (RGDS) and cyclo[RGDfK(CX-)] (c(RGDfK)) peptides (X = 6-aminocaproic acid; ϵ-Acp) were purchased from Peptide Institute, Inc. (Japan). The PEG–PLys block copolymer (PEG; 12 000 g/mol, polymerization degree of PLys segment; 73) was synthesized as previously reported (*13*). A micro BCA protein assay reagent kit was purchased from Pierce (Rockford, IL). The Luciferase assay kit was a product of Promega (Madison, WI). Plasmid pCAcc+Luc coding for firefly luciferase under the control of the CAG promoter was provided by the RIKEN Gene Bank (Japan), amplified in competent DH5α *Escherichia coli*, and then purified using a HiSpeed Plasmid MaxiKit purchased from QIAGEN Sciences Co., Inc. (Germany). FITC-labeled monoclonal antibodies against $\alpha_v\beta_3$ integrin, $\alpha_v\beta_5$ integrin, and mouse IgG were purchased from Cosmo Bio Co., Ltd. (Japan). QuantiLum recombinant luciferase was purchased from Promega (Madison, WI).

Measurements. Gel permeation chromatography (GPC) measurements were carried out using a TOSOH HLC-8220 equipped with TSKgel columns (G4000PWXL and G3000PWXL). The internal refractive index (RI) was used for detection of the polymer. DMF with 10 mM LiCl was used as an eluent at a flow rate of 0.8 mL min^{-1} at 40 °C. IR was measured with an IR Report-100 spectrometer (JASCO, Tokyo, Japan). ^{1}H NMR spectra were obtained with a JEOL EX300 spectrometer (JEOL, Tokyo, Japan). Chemical shifts are reported in ppm relative to the residual protonated solvent resonance.

Synthesis of RGDS–PEG–PLys 5a and c(RGDfK)–PEG–PLys 5b (Scheme 1). *Acetal-PEG-NH$_2$ 2.* A THF solution of 3,3-diethoxypropanol (0.16 mL, 1 mmol) and potassium naphthalene (2.7 mL, 0.90 mmol) were mixed in THF (75 mL) to form potassium 3,3-diethoxypropanolate (PDP) as previously reported (*14*). After the mixture was stirred for 10 min, liquid EO (13.5 mL, 270 mmol) chilled below 0 °C was added to the solution with additional stirring at room temperature (r.t.) for 2 days. The reactant polymer was isolated by precipitation into diethyl ether and lyophilized from benzene to obtain acetal-PEG-OH (12.65 g, quant). Acetal-PEG-OH (6.01 g, 0.50 mmol) was then dissolved in THF (40 mL), followed by the addition of TEA (0.32 mL, 2.25 mmol). Subsequently, the solution was slowly added dropwise into MsCl (0.12 mL, 1.5 mmol) in THF (20 mL) and stirred at 0 °C for 2 h. The solution was poured into diethyl ether to precipitate acetal-PEG-OMs **1**. The recovered acetal-PEG-OMs **1** was dissolved in 25% ammonia solution (500 mL) and stirred at r.t. for 4 days. The volume of the solution was concentrated to 50 mL by evaporation and dialyzed sequentially against 0.125% ammonia solution and distilled water, followed by lyophilization to obtain acetal-PEG-NH$_2$ **2** (5.40 g, 90%).

Acetal-PEG–PLys(TFA) 3. N^{ϵ}-Trifluoroacetyl-L-lysine *N*-carboxyanhydride (Lys(TFA)-NCA) (3.59 g, 13.39 mmol, 80 equiv to **2**) prepared according to the protocol described in the literature (*15*) in DMF (40 mL) was added to acetal-PEG-NH$_2$ **2** (2.01 g, 167.5 μmol) in DMF (20 mL) and stirred at 40 °C for 2 days. The polymerization was monitored by IR. The reactant polymer was precipitated into AcOEt/hexane (4:6) and lyophilized in dioxane to obtain acetal-PEG–PLys(TFA) **3** (4.08 g, 73%).

Acetal-PEG–PLys 4. NaOH solution (1 N, 4 mL) was added to acetal-PEG–PLys(TFA) **3** (500 mg, 17.77 μmol) in MeOH (40 mL) and stirred at 40 °C for 24 h. The reacted polymer was purified by dialysis sequentially against 10 mM PBS solution (pH 7.0) and distilled water and lyophilized to obtain acetal-PEG–PLys **4** (498 mg, quant).

*RGDS–PEG–PLys **6a** and c(RGDfK)–PEG–PLys **6b**.* Conjugation of the peptide into the PEG terminus of PEG–PLys was performed through thiazolidine ring formation using RGDS or c(RGDfK) peptide. RGDS–PEG–PLys **6a** was synthesized according to the typical procedure, as follows: Acetal-PEG–PLys **4** (39.1 mg, 1.64 μmol) was added to RGDS (15.2 mg, 16.4 μmol) in 0.2 M AcOH buffer (pH 4.0, 8 mL) and stirred at room temperature for 5 days. The reacted polymer was purified by dialysis sequentially against 10 mM PBS solution (pH 7.0) and distilled water and lyophilized to obtain RGDS–PEG–PLys **6a** (35.4 mg, 86%). Conjugation of the c(RGDfK) to acetal-PEG–PLys **4** was carried out in a similar way, e.g., c(RGDfK) (7.4 mg, 9.03 μmol) and acetal-PEG–PLys **4** (30.0 mg, 1.26 μmol) were used to obtain c(RGDfK)–PEG–PLys **6b** (26.6 mg, 87%).

Preparation of Polyplex Micelles. Each block copolymer and pDNA was dissolved separately in 10 mM Tris-HCl buffer (pH 7.4). The polymer solution in varying concentrations was added to a twice-excess volume of pDNA solution to form polyplex micelles with different compositions. The final pDNA concentration was adjusted to 33.3 or 50 μg/mL. The resulting solution was kept at r.t. overnight. The N/P ratio was defined as the residual molar ratio of the amino groups of PLys units to the phosphate groups of pDNA.

Ethidium Bromide Exclusion Assay. Polyplex micelle solutions (50 μg pDNA/mL) prepared at various N/P ratios were

Scheme 1. Syntheses of RGDS−PEG−PLys 6a and c(RGDfK)−PEG−PLys 6b

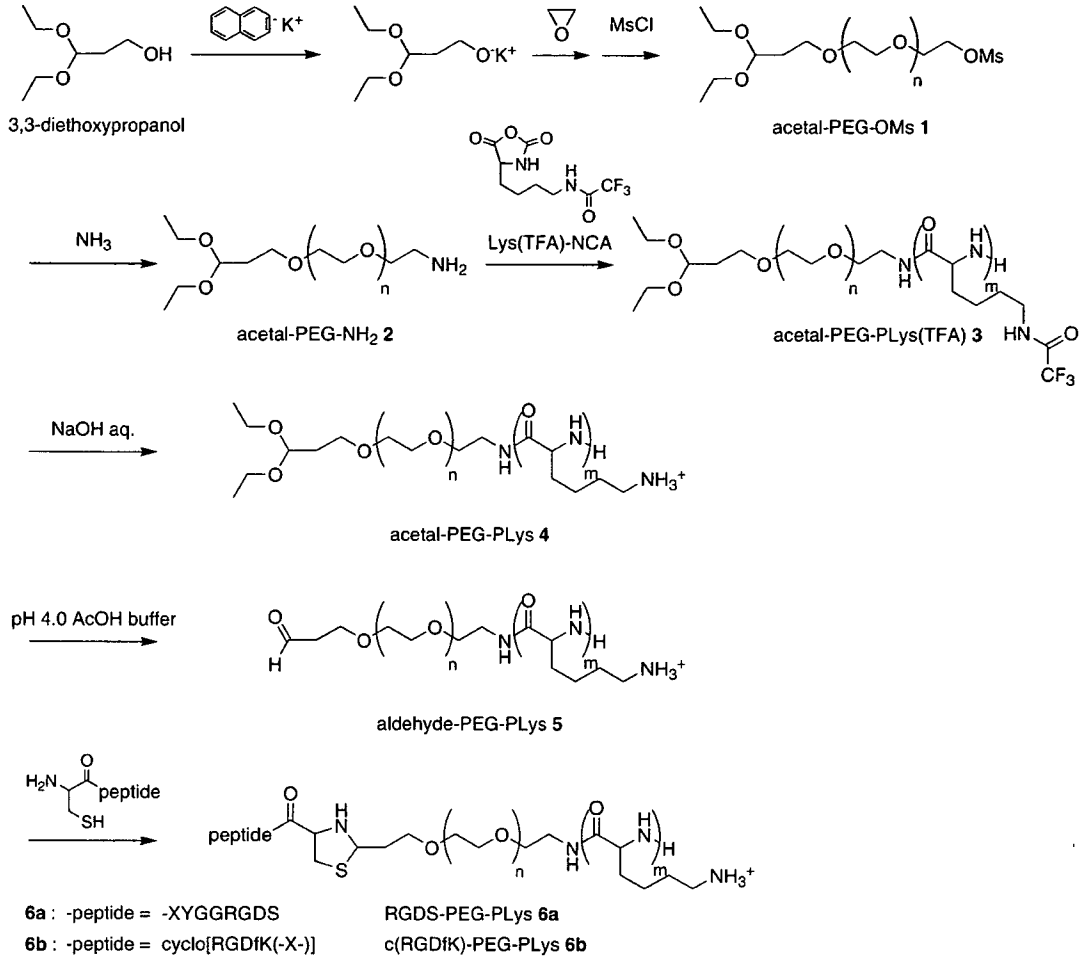

adjusted to contain 10 μg pDNA/mL with 2.5 μg ethidium bromide (EtBr)/mL and 150 mM NaCl by adding 10 mM Tris-HCl solution (pH 7.4) containing EtBr and NaCl. The solutions were kept at r.t. overnight. The fluorescence intensity of the sample solutions at 590 nm (excitation wavelength: 365 nm) was measured at 25 °C using a spectrofluorometer (ND-3300, NanoDrop, Wilmington, DE). The fluorescence intensity of naked pDNA was set at 100% and measured against a background of EtBr without pDNA.

Dynamic Light Scattering Measurement. The size of the polyplex micelles was evaluated by dynamic light scattering (DLS) using Nano ZS (ZEN3600, Malvern Instruments, Ltd., UK). A He−Ne ion laser (633 nm) was used as the incident beam. Polyplex micelle solutions (50 μg pDNA/mL) with an N/P = 2 were adjusted to a concentration of 10 μg pDNA/mL. The data obtained at a detection angle of 173 ° at 25 °C were analyzed by a cumulant method to obtain the hydrodynamic diameters and polydispersity indices (μ/Γ^2) of the micelles. The results reported are expressed as the mean values (±SEM) of three experiments.

ζ-Potential Measurement. The ζ-potential of polyplex micelles was evaluated by the laser-doppler electrophoresis method using Nano ZS with a He−Ne ion laser (633 nm). Sample solutions similar to those used for the DLS measurements were prepared. The ζ-potential measurements were carried out at 25 °C. A scattering angle of 17° was used in these measurements. The results are expressed as the mean values (±SEM) of three experiments.

Detection of $\alpha_v\beta_3$ and $\alpha_v\beta_5$ Integrin Receptors. 293T cells and HeLa cells were detached by pipetting and by harvesting with trypsin, respectively. Both types of cells were washed twice with PBS. The 1 × 10^6 cells and FITC-labeled antibody against $\alpha_v\beta_3$ or $\alpha_v\beta_5$ integrin (2 μg) were resuspended in 100 μL of Dulbecco's Modified Eagle Medium (DMEM) (containing 10% serum) and incubated on ice for 1 h in the dark. The cells were washed three times with cold medium and, after being resuspended in PBS, were analyzed using a flow cytometer (EPICS XL, Beckman Coulter, Inc.). The cytometric data were analyzed using EXPO32 software (Beckman Coulter, Inc., Fullerton, CA).

Transfection. HeLa and 293T cells were respectively seeded on 24-well culture plates (10 000 cells/well) and incubated overnight in 500 μL of DMEM containing 10% serum. After the medium was replaced with fresh medium, 20 μL of polyplex solution (50 μg pDNA/mL, N/P = 2) was applied to each well. The amount of pDNA was adjusted to 1 μg per well. After incubation for various lengths of time, the medium was replaced with 500 μL of fresh medium, followed by reincubation. The reincubation time was adjusted so the total incubation time would be 48 h. The luciferase gene expression was then evaluated based on the intensity of the photoluminescence using the Luciferase assay kit and a Luminometer (Lumat LB9507, BERTHOLD, Germany). The amount of protein in each well was concomitantly determined using a Micro BCA protein assay reagent kit. The relative light units were converted into the absolute amount of luciferase (ng) using a standard curve calibrated with recombinant luciferase (QuantiLum, Promega). One nanogram of luciferase corresponded to 9.1 × 10^7 RLU in our experiments; this was defined as the conversion factor.

Analysis of Cellular Uptake of Polyplex Micelles. pDNA was labeled with fluorescein as previously reported (*4*). Briefly,

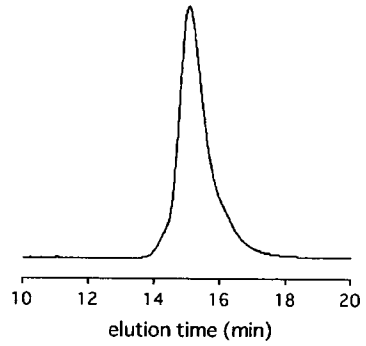

Figure 1. Gel permeation chromatogram of acetal-PEG−PLys(TFA) **3** (instrument TOSOH HLC-8220, detector RI, columns TSKgel G4000PWXL and G3000PWXL, eluent DMF with 10 mM LiCl, flow rate 0.8 mL min^{-1}, temperature 40 °C).

pDNA was labeled using a Label IT Nucleic Acid Labeling Kit (Mirus, Madison, WI). HeLa cells were seeded on six-well culture plates (100 000 cells/well) and incubated overnight in 1 mL of DMEM containing 10% serum. After the medium was replaced with fresh medium, 90 μL of polyplex solution (33.3 μg fluorescein-labeled pDNA/mL, N/P = 2) was applied to each well. The amount of fluorescein-labeled pDNA was adjusted to 3 μg per well. After various periods of incubation, the medium was removed and the cells were washed twice with PBS. After detachment by trypsin, the cells were resuspended in PBS and analyzed using the flow cytometer.

Confocal Laser Scanning Microscope (CLSM) Observation. pDNA was labeled with Cy5 in the same manner as fluorescein using the Label IT Nucleic Acid Labeling Kit. HeLa cells (30 000 cells) were seeded on a 35-mm glass base dish (Iwaki, Japan) and incubated overnight in 1 mL of DMEM containing 10% serum. After the medium was replaced with fresh medium, 90 μL of polyplex solution containing 3 μg Cy5-labeled pDNA (N/P = 2) was applied to a glass dish. After 3 h incubation, the medium was removed and the cells were washed twice with PBS. The intracellular distributions of the polyplex micelles were observed by CLSM following acidic late endosome and lysosome staining with LysoTracker Green (Molecular Probes, Eugene, OR) and nuclear staining with Hoechst 33342 (Dojindo Laboratories, Japan). The CLSM observation was performed using LSM 510 (Carl Zeiss, Germany) with a 63× objective (C-Apochromat, Carl Zeiss, Germany) at excitation wavelengths of 488 nm (Ar laser), 633 nm (He−Ne laser), and 710 nm (Mai Tai laser) for fluorescein, Cy5, and Hoechst 33342, respectively.

RESULTS

Synthesis of Peptide-Conjugated PEG−PLys (Scheme 1). The synthesis of acetal-PEG-OMs **1** has been previously reported (*14*). Briefly, PDP from 3,3-diethoxypropanol and potassium naphthalene initiated the anionic polymerization of EO to form acetal-PEG-OH (M_n 11 825, M_w 12 089, M_w/M_n 1.02), followed by the mesylation of alcohol using MsCl to obtain acetal-PEG-OMs **1**. Acetal-PEG-NH_2 **2** was then synthesized by amination of acetal-PEG-OMs **1** using ammonia solution and was confirmed to be unimodal with a narrow molecular weight distribution (M_w/M_n 1.03). Polymerization of Lys(TFA)-NCA using acetal-PEG-NH_2 **2** as an initiator led to the formation of acetal-PEG−PLys(TFA) **3**. A GPC of the obtained acetal-PEG−PLys(TFA) **3** showed a single peak with a narrow molecular weight distribution (M_w/M_n 1.12) (Figure 1). From the peak intensity ratio of the methylene protons of PEG (OCH_2CH_2, δ = 3.6 ppm) and the methylene protons of Lys(TFA) ($CH_2CH_2CH_2CH_2NH$, δ = 1.4, 1.5, 1.9, and 3.2 ppm) measured by ^{1}H NMR, the polymerization degree (DP) of Lys-

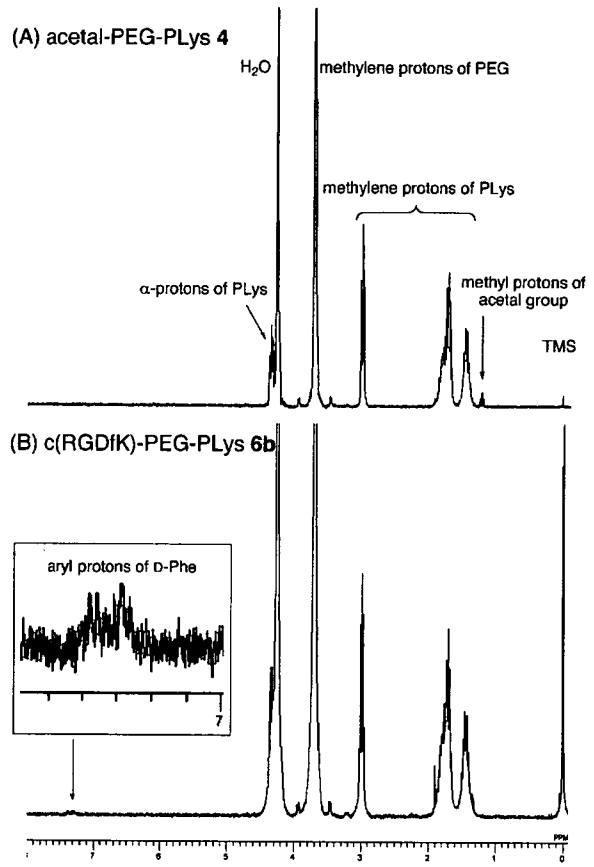

Figure 2. ^{1}H NMR spectra of acetal-PEG−PLys **4** (A) and c(RGDfK)−PEG−PLys **6b** (B) in D_2O at 80 °C.

(TFA) was calculated to be 70 (data not shown). Acetal-PEG−PLys **4** was then quantitatively obtained by the deprotection of acetal-PEG−PLys(TFA) **3** under basic conditions. From the ^{1}H NMR spectrum, the acetal group (CH_3CH_2O, δ = 1.2 ppm) was confirmed to be almost intact without converting to an aldehyde group (Figure 2). The DP of Lys was calculated to be 72 from the peak intensity ratio of the methylene protons of PEG (OCH_2CH_2, δ = 3.6 ppm) and the methylene protons of PLys ($CH_2CH_2CH_2CH_2NH_3$, δ = 1.4, 1.7, and 3.0 ppm) (Figure 2). The DP of acetal-PEG−PLys(TFA) **3** and acetal-PEG−PLys **4** were almost identical, indicating that main chain cleavage under the deprotection reaction was negligible.

Conjugation of peptide ligands into the PEG terminus of acetal-PEG−PLys **4** was achieved through the formation of a thiazolidine ring. The acetal group was deprotected under acidic conditions to an aldehyde group, giving aldehyde-PEG−PLys **5**. The aldehyde group is known to react with cysteine to form a stable thiazolidine ring (*16*). In this study, CXYGGRGDS (RGDS) and cyclo[RGDfK(CX-)] (c(RGDfK)), having an N-terminal cysteine residue (C: L-Cys), were reacted with acetal-PEG−PLys **4** under mild acidic conditions (pH 4.0) to prepare the peptide-conjugated PEG−PLys through thiazolidine formation. Note that Schiff base formation due to the reaction of the aldehyde and primary amino groups of the PLys segment was prohibited under the acidic conditions because of the complete protonation of the primary amino groups. The methyl protons of the acetal group (δ = 1.2 ppm) completely disappeared with the appearance of protons assigned to the aromatic rings of L-tyrosine (Y: L-Tyr:) (δ = 6.9 and 7.1 ppm) in the RGDS and D-phenylalanine (f: D-Phe) (δ = 7.3 and 7.4 ppm) in the c(RGDfK) (Figure 2). Based on the peak intensity ratios of the aromatic ring protons of peptide ligands and the methylene

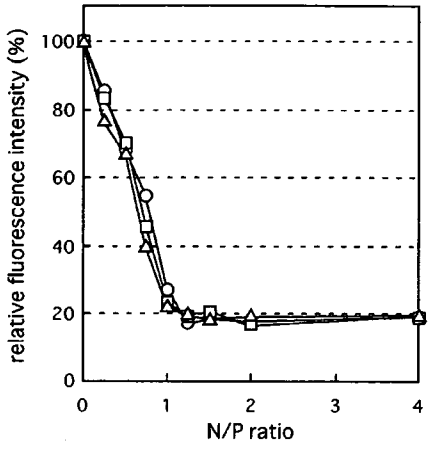

Figure 3. Ethidium bromide exclusion assays of PEG–PLys (open circle), RGDS–PEG–PLys (open square), and c(RGDfK)–PEG–PLys (open triangle). Fluorescence measurements were carried out as described in the Experimental Procedures.

Table 1. Size and ζ-Potentials of Polyplex Micelles

sample	cumulant diameter (nm)/ polydispersity index (μ/Γ^2)	ζ-potential (mV)
PEG–PLys	124 ± 0.27/0.158 ± 0.014	−0.19 ± 0.195
RGDS–PEG–PLys	124 ± 0.88/0.177 ± 0.012	1.12 ± 0.349
c(RGDfK)–PEG–PLys	125 ± 1.00/0.166 ± 0.006	0.68 ± 0.238

protons of PEG (OCH_2CH_2, δ = 3.6 ppm), the introduction rates of peptide ligands were determined to be 100% in the RGDS–PEG–PLys **6a** and 66% in the c(RGDfK)–PEG–PLys **6b**.

Formation of Polyplex Micelles. Ethidium bromide (EtBr) is known to form an intercalating complex with double helical polynucleotides and subsequently show a striking enhancement of its fluorescence intensity (*17*). This enhancement is quenched by the formation of a complex between DNA and cationic components, because cationic components prevent EtBr from intercalating into the double-strand DNA. Thus, EtBr exclusion assay is frequently utilized to estimate the degree of pDNA condensation in the complex with a catiomer (*18*, *19*). As shown in Figure 3, as the N/P ratio increased, the fluorescence intensity in all the polyplex micelles decreased correspondingly and leveled off at around N/P = 1.25. This result indicates that the degree of pDNA condensation was not influenced by the introduction of peptide ligands. Table 1 summarizes the cumulant diameters and ζ-potentials of the polyplex micelles at N/P = 2. The cumulant diameters of all the micelles were approximately 125 nm with a moderate polydispersity index between 0.15 and 0.18. There was no change in the particle size because of the introduction of peptide ligands. Also, the ζ-potentials of all the polyplex micelles were approximately 0 mV. As previously reported (*5*, *18*), the PEG palisade surrounding the complex shields the charge of the micelles to maintain a very small absolute value in the ζ-potential even in the region of N/P > 1. All of the results of the EtBr assay, DLS analysis, and ζ-potential measurement suggest that the characteristics of the three types of polyplex micelles (PEG–PLys, RGDS–PEG–PLys, and c(RGDfK)–PEG–PLys) were quite similar regardless of the introduction of the peptide ligands.

Detection of $\alpha_v\beta_3$ and $\alpha_v\beta_5$ Integrin Receptors. To evaluate the expression of integrin receptors on the cell surface, flow cytometric analysis of 293T and HeLa cells was carried out using FITC-labeled antibodies (Figure 4). Flow cytometric analysis revealed that the 293T cells expressed almost no $\alpha_v\beta_3$ integrin and a slight amount of $\alpha_v\beta_5$ integrin, while the HeLa cells expressed a considerably higher amount of $\alpha_v\beta_3$ and $\alpha_v\beta_5$ integrins than the 293T cells. These results implied that HeLa cells might show a higher uptake of the cyclic RGD peptide-conjugated polyplex micelles than 293T cells through integrin-mediated endocytosis.

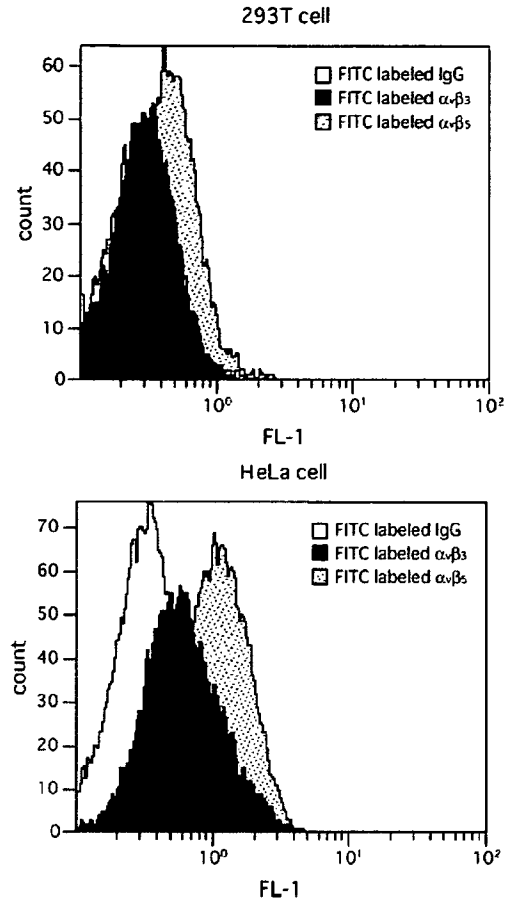

Figure 4. Flow cytometric analysis of integrin expression on 293T cells (left) and HeLa cells (right).

Transfection. *In vitro* TE of polyplex micelles was evaluated for 293T cells and HeLa cells at varying transfection times (Figure 5). PEG–PLys/pDNA micelles without the peptide ligand and RGDS–PEG–PLys/pDNA micelles with a linear RGD peptide ligand were used as controls. RGD peptide is the adhesion motif of extracellular matrix proteins for the various types of integrins (*20*, *21*). The linear RGD peptide showed a binding affinity for $\alpha_v\beta_3$ integrin approximately 1/1000 of that of the cyclic RGD peptide (*22*). In the transfection experiment using 293T cells, there were no differences in the TE of the three types of micelles at any of the transfection times. This finding is consistent with the observation that 293T cells showed low integrin expression (Figure 4). On the other hand, in the transfection experiment using HeLa cells, c(RGDfK)–PEG–PLys micelles achieved a significantly higher TE than PEG–PLys and RGDS–PEG–PLys micelles. It is reasonable to assume that HeLa cells might efficiently recognize c(RGDfK) ligands on the micelle through $\alpha_v\beta_3$ and $\alpha_v\beta_5$ integrins expressed on their surface. Nevertheless, the TE of linear RGD peptide-conjugated micelles toward HeLa cells was comparable to that of the micelles without any ligand, suggesting that the binding affinity of the linear RGD peptide for the integrins might be insufficient to increase the TE.

Analysis of Cellular Uptake of Polyplex Micelles. The cellular uptake of the micelles into the HeLa cells was evaluated by a flow cytometer using fluorescein-labeled pDNA-incorporated micelles with varying incubation times (Figure 6). The amount of the uptake was always higher for c(RGDfK)–PEG–

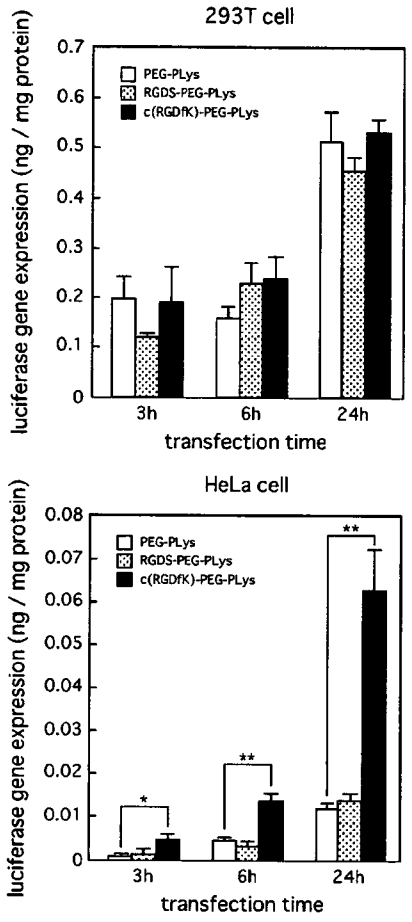

Figure 5. Effect of cell lines and transfection time on gene expression. 293T cells (left) and HeLa cells (right) were transfected with PEG–PLys, RGDS–PEG–PLys, and c(RGDfK)–PEG–PLys micelles prepared at N/P = 2 in a medium containing 10% serum. The data are the mean ± SEM, $n = 4$. $P^* < 0.05$ and $P^{**} < 0.01$.

PLys micelles than for PEG–PLys micelles at each incubation time, which suggests that the specific interaction of the cyclic RGD peptide with integrin receptors on the HeLa cells contributed to the uptake amount. In 24 h incubation, the amount of c(RGDfK)–PEG–PLys micelles that were taken up was 1.6 times the amount of PEG–PLys micelles taken up (Figure 6B). Nevertheless, c(RGDfK)–PEG–PLys micelles revealed an even higher TE of approximately 5 times that of the PEG–PLys micelles (Figure 5). This implied that other factors besides the enhanced uptake might also play a role in the enhanced TE observed for HeLa cells challenged with c(RGDfK)–PEG–PLys micelles.

Intracellular Distribution of Polyplex Micelles. The intracellular distribution of polyplex micelles was investigated by CLSM using Cy5-labeled pDNA-incorporated micelles with 3 h incubation, and typical images from this investigation are shown in Figure 7. A large fraction of the Cy5-labeled pDNA was still distributed near the cell membrane for the cells challenged with PEG–PLys polyplex micelles (Figure 7A). Alternatively, an appreciable accumulation of the Cy5-labeled pDNA in the perinuclear regions was observed for the cells challenged with c(RGDfK)–PEG–PLys polyplex micelles (Figure 7B). Further detailed observation using LysoTracker, which labels acidic late endosome and lysosome, revealed that the majority of c(RGDfK)–PEG–PLys polyplex micelles were localized in the acidic compartments as indicated by the yellow color in the merged fluorescence image of the Cy5-labeled pDNA (red) and LysoTracker (green), yet a fraction that did not co-localize with LysoTracker was also observed, suggesting that at least some of the polyplex micelles in the perinuclear regions may be located in a site other than the lysosomes.

DISCUSSION

There are many barriers to achieve effective transfection using nonviral gene vectors. Stability in the bloodstream and specific cellular uptake by the target tissues and organs are major obstacles, especially for *in vivo* gene delivery. Polyplex micelles with PEG as a hydrophilic shell layer have been shown to achieve an increased retention time in the bloodstream (*5*), and they are promising candidates for vectors that can be used for *in vivo* gene delivery. Also, the introduction of targetable ligands onto polyplex micelles has been reported, and some of the ligand-installed polyplex micelles have been demonstrated to be effective both in *in vivo* as well as *in vitro* transfection (*6*–*8*). The ligands on polyplex micelles may facilitate their internalization into the target cells, thus increasing the TE. A number of studies have aimed to find suitable ligands for this purpose (*23*), and cyclic RGD peptides have been highlighted as one of the promising candidates (*7*). Cyclic RGD peptides are well-known to selectively recognize $\alpha_v\beta_3$ and $\alpha_v\beta_5$ integrins, which are overexpressed in angiogenic endothelial cells in tumors. Therefore, a targetable gene delivery system equipped with a cyclic RGD peptide as the ligand may be useful for antiangiogenic therapy for tumors (*24*, *25*).

In this study, to construct polyplex micelles showing integrin-mediated gene transfection, the novel synthetic route of a block copolymer with a c(RGDfK) peptide ligand was exploited as summarized in Scheme 1. The acetal group may be converted to an aldehyde group under acidic conditions. Thus, the TFA group was selected to protect the primary amino group of the lysine units, because it can be removed under basic conditions without any conversion of acetal groups to aldehyde groups. The introduction of peptide ligands was then carried out under mild acidic conditions with good yields in a one-pot reaction involving the conversion of acetal groups to aldehyde groups and the subsequent conjugation of the ligand through the formation of a thiazolidine ring as seen in Scheme 1. In this way, various peptide ligands having a cysteine end group (Cys-peptide) may be readily introduced into the block copolymer. Moreover, this type of conjugation reaction between aldehyde and Cys-peptide occurs selectively even in the presence of primary amines, because the formation of a Schiff base between a primary amine and an aldehyde is reversible and thus sensitive to pH, while the thiazolidine ring formation between the N-terminal cysteine and aldehyde is an irreversible reaction. This reaction is available for the introduction of various ligands into the block copolymer, not only peptides but also other ligand molecules possessing an N-terminal cysteine.

Indeed, as confirmed by the NMR spectra shown in Figure 2, the c(RGDfK) peptide, which can peculiarly recognize $\alpha_v\beta_3$ and $\alpha_v\beta_5$ integrins, was successfully introduced into the PEG terminus of the PEG–PLys block copolymer as a targetable ligand molecule. The c(RGDfK)–PEG–PLys/pDNA micelle achieved a higher TE compared to nontargetable PEG–PLys and RGDS–PEG–PLys micelles against HeLa cells, which express an appreciable amount of $\alpha_v\beta_3$ and $\alpha_v\beta_5$ integrins. In contrast, there was no difference in TE among these three types of polyplex micelles against 293T cells, which show a limited expression of $\alpha_v\beta_5$ integrin, but no expression of $\alpha_v\beta_3$ integrin. This result is consistent with a previous report which found that the $\alpha_v\beta_3$ integrin has an approximately 10-times higher binding affinity for the cyclic RGD peptide than the $\alpha_v\beta_5$ integrin (*26*), which suggests that the $\alpha_v\beta_3$ integrin may be involved in an increased TE against HeLa cells by means of the c(RGDfK)–PEG–PLys/pDNA micelle. Flow cytometric analysis (Figure

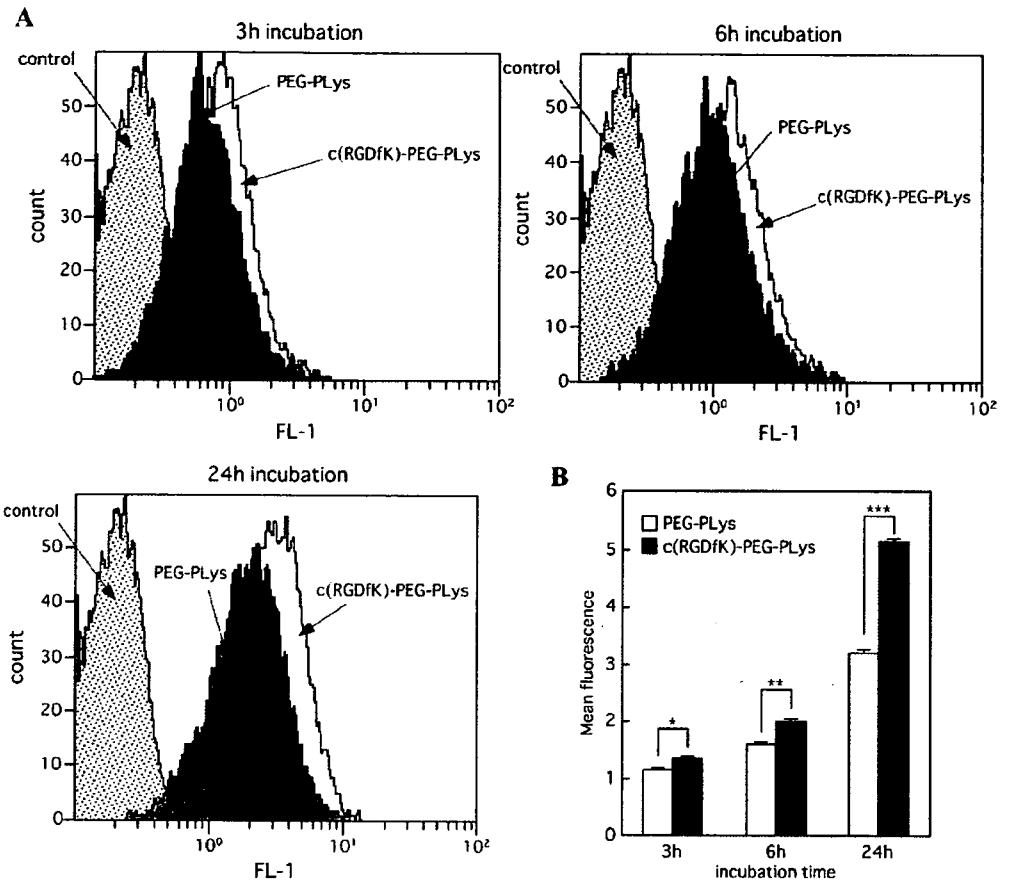

Figure 6. Cellular uptake of polyplex micelles. PEG−PLys and c(RGDfK)−PEG−PLys micelles loaded with fluorescein-labeled pDNA were applied to HeLa cells with varying incubation times. (A) Flow cytometric histogram profiles of time-dependent change in fluorescence intensity. (B) Mean fluorescence intensity at each incubation time. The data are the mean ± SEM, $n = 3$. $P^* < 0.05$, $P^{**} < 0.01$, and $P^{***} < 0.001$.

6) also suggests that the enhanced uptake of the c(RGDfK)−PEG−PLys/pDNA micelle might contribute to an increased TE against HeLa cells. Interestingly, the difference in the uptake ratio against the HeLa cells between the c(RGDfK) micelle and the ligand-free micelle became more significant with increased incubation time as seen in Figure 6. Integrin receptors are known to recycle to the plasma membrane through an endocytic cycle every 15−40 min (*27*). Consequently, this fast recycle of integrins might contribute to the facilitated uptake of the c(RGDfK) micelle into the HeLa cells in comparison with the ligand-free micelle. Nevertheless, as can be seen from Figures 5 and 6B, the uptake ratio is not simply correlated in a time-dependent manner with the TE. The ligand effect appeared to be more significant in the TE than in the uptake ratio, particularly after a prolonged time period such as 24 h. This result led us to assume that the c(RGDfK) ligand may also affect intracellular trafficking of the polyplex micelles. Indeed, a CLSM observation of HeLa cells challenged with polyplex micelles revealed a substantial difference in intracellular distribution between the PEG−PLys and c(RGDfK)−PEG−PLys micelles (Figure 7). In the cells challenged with the PEG−PLys polyplex micelle, a majority of pDNA was still distributed near the cell membrane, whereas in the same time frame of 3 h the cells with the c(RGDfK)−PEG−PLys polyplex micelle showed an appreciable accumulation of pDNA in the perinuclear region. It is noteworthy that a definite fraction of pDNA (colored red) in the perinuclear region did not co-localize with LysoTracker (colored green), suggesting that this fraction may be located in a compartment other than the acidic late endosome and lysosome. The $\alpha_v\beta_3$ integrin receptors have been reported to pass rapidly through the early endosomes, arriving at the perinuclear compartments approximately 30 min after internalization (*28*). Recent reports have shown an active transport pathway for a nonviral gene delivery system (*29*, *30*), in which microtubule-associated motor proteins have contributed to a rapid perinuclear accumulation of the polyplex within minutes after transfection. Also, recent studies have revealed that polyplexes in the perinuclear region but not in the acidic compartments significantly contribute to the effective transfection (*31*, *32*). These phenomena are consistent with our observation of a partial accumulation of the c(RGDfK)−PEG−PLys micelle in the perinuclear sites but outside of the acidic compartments, suggesting that the enhancement of the TE of the polyplex micelle by the introduction of cyclic RGD peptide ligands might be due not only to the enhanced uptake but also to the change in the intracellular trafficking route directed to the nucleus. It is likely that the micelle fraction distributed in nonacidic compartments near the nucleus may efficiently internalize into the nucleus when the cells are in the dividing phase, thus contributing to the increase in the transfection. Although the effective transport of the PLys-based polyplex micelles from the isolated compartment into the cytoplasm remains an issue because of inefficiency in the PLys function of facilitating the endosome-escaping step, the conjugation of c(RGDfK) ligands onto the polyplex micelle surface has great potential to improve the TE through modulated intracellular trafficking.

In conclusion, a successful synthetic route involving block copolymers conjugated with peptidyl ligands through thiazolidine ring formation was developed in this study. Cyclic RGD peptide-conjugated polyplex micelles showed an increased TE against HeLa cells possessing $\alpha_v\beta_3$ and $\alpha_v\beta_5$ integrins because

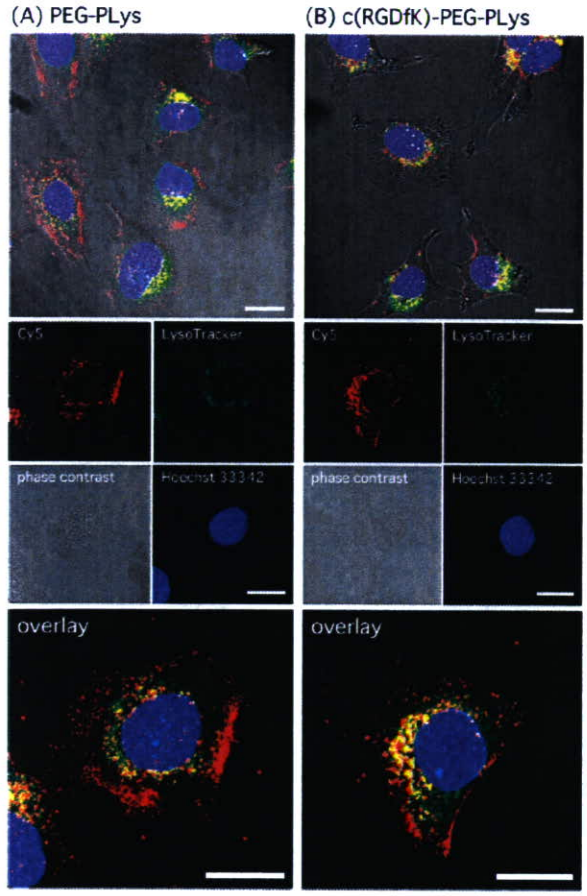

Figure 7. Intracellular distribution of pDNA challenged by the polyplex micelles. PEG−PLys and c(RGDfK)−PEG−PLys micelles loaded with Cy5-labeled pDNA (red) were incubated with HeLa cells for 3 h. The CLSM observation was performed using a 63× objective. The cell nuclei were stained with Hoechst 33342 (blue), and the acidic late endosome and lysosome were stained with LysoTracker Green (green). The scale bar represents 20 μm.

of enhanced uptake and a possible change in the route of intracellular trafficking. These results indicate that the introduction of various peptide ligands including c(RGDfK) peptide into the block copolymers is feasible and could eventually allow the construction of targetable polyplex micelles that are useful for site-specific gene therapy through a systemic route.

ACKNOWLEDGMENT

We thank Ms. K. Date (The University of Tokyo) and Ms. J. Kawakita (The University of Tokyo) for technical assistance. This work was financially supported in part by the Core Research Program for Evolutional Science and Technology (CREST) from Japan Science and Technology Corporation (JST) and the Project on the Materials Development for Innovative NanoDrug Delivery Systems from the Ministry of Education, Culture, Sports, Science and Technology (MEXT), Japan.

LITERATURE CITED

(1) Pedroso de Lima, M. C., Simoes, S., Pires, P., Faneca, H., and Düzgunes, N. (2001) Cationic lipid-DNA complexes in gene delivery: from biophysics to biological applications. *Adv. Drug Delivery Rev. 47*, 277−294.

(2) Merdan, T., Kopecek, J., and Kissel, T. (2002) Prospects for cationic polymers in gene and oligonucleotide therapy against cancer. *Adv. Drug Delivery Rev. 54*, 715−758.

(3) Kakizawa, Y., and Kataoka, K. (2002) Block copolymer micelles for delivery of gene and related compounds. *Adv. Drug Delivery Rev. 54*, 203−222.

(4) Itaka, K., Harada, A., Nakamura, K., Kawaguchi, H., and Kataoka, K. (2002) Evaluation by fluorescence resonance energy transfer of the stability of nonviral gene delivery vectors under physiological conditions. *Biomacromolecules 3*, 841−845.

(5) Harada-Shiba, M., Yamauchi, K., Harada, A., Takamisawa, I., Shimokado, K., and Kataoka, K. (2002) Polyion complex micelles as vectors in gene therapy-pharmacokinetics and in vivo gene transfer. *Gene Ther. 9*, 407−414.

(6) Wakebayashi, D., Nishiyama, N., Yamasaki, Y., Itaka, K., Kanayama, N., Harada, A., Nagasaki, Y., and Kataoka, K. (2004) Lactose-conjugated polyion complex micelles incorporating plasmid DNA as a targetable gene vector system: their preparation and gene transfecting efficiency against cultured HepG2 cells. *J. Controlled Release 95*, 653−664.

(7) Suh, W., Han, S.-O., Yu, L., and Kim, S. W. (2002) An angiogenic, endothelial-cell-targeted polymeric gene carrier. *Mol. Ther. 6*, 664−672.

(8) Ogris, M., Walker, G., Blessing, T., Kircheis, R., Wolschek, M., and Wagner, E. (2003) Tumor-targeted gene therapy: strategies for the preparation of ligand-polyethylene glycol-polyethylenimine/DNA complexes. *J. Controlled Release 91*, 173−181.

(9) Miyata, K., Kakizawa, Y., Nishiyama, N., Yamasaki, Y., Watanabe, T., Kohara, M., and Kataoka, K. (2005) Freeze-dried formulations for in vivo gene delivery of PEGylated polyplex micelles with disulfide crosslinked cores to the liver. *J. Controlled Release 109*, 15−23.

(10) Haubner, R., Gratias, R., Diefenbach, B., Goodman, S. L., Jonczyk, A., and Kessler, H. (1996) Structural and functional aspects of RGD-containing cyclic pentapeptides as highly potent and selective integrin $\alpha_v\beta_3$ antagonist. *J. Am. Chem. Soc. 118*, 7461−7472.

(11) Brooks, P. C., Clark, R. A. F., and Cheresh, D. A. (1994) Requirement of vascular integrin $\alpha_v\beta_3$ for angiogenesis. *Science 264*, 569−571.

(12) Akiyama, Y., Harada, A., Nagasaki, Y., and Kataoka, K. (2000) Synthesis of poly(ethylene glycol)-*block*-poly(ethylenimine) possessing an acetal group at the PEG end. *Macromolecules 33*, 5841−5845.

(13) Harada, A., and Kataoka, K. (1995) Formation of polyion complex micelles in an aqueous milieu from a pair of oppositely charged block copolymers with poly(ethylene glycol) segments. *Macromolecules 28*, 294−299.

(14) Nagasaki, Y., Kutsuna, T., Iijima, M., Kato, M., and Kataoka, K. (1995) Formyl-ended heterobifunctional poly(ethylene oxide): synthesis of poly(ethylene oxide) with a formyl group at one end and a hydroxyl group at the other end. *Bioconjugate Chem. 6*, 231−233.

(15) Poche, D. S., Moore, M. J., and Bowles, J. L. (1999) An unconventional method for purifying *N*-carboxyanhydride derivatives of γ-alkyl-L-glutamates. *Synth. Commun. 29*, 843−854.

(16) Zhang, L., Torgerson, T. R., Liu, X.-Y., Timmons, S., Colosia, A. D., Hawiger, J., and Tam, J. P. (1998) Preparation of functionally active cell-permeable peptides by single-step ligation of two peptide modules. *Proc. Natl. Acad. Sci. U.S.A. 95*, 9184−9189.

(17) LePecq, J.-B., and Paoletti, C. (1967) A fluorescent complex between ethidium bromide and nucleic acids. *J. Mol. Biol. 27*, 87−106.

(18) Itaka, K., Yamauchi, K., Harada, A., Nakamura, K., Kawaguchi, H., and Kataoka, K. (2003) Polyion complex micelles from plasmid DNA and poly(ethylene glycol)-poly(L-lysine) block copolymer as serum-tolerable polyplex system: physicochemical properties of micelles relevant to gene transfection efficiency. *Biomaterials 24*, 4495−4506.

(19) Wakebayashi, D., Nishiyama, N., Itaka, K., Miyata, K., Yamasaki, Y., Harada, A., Koyama, H., Nagasaki, Y., and Kataoka, K. (2004) Polyion complex micelles of pDNA with acetal-poly(ethylene glycol)-poly(2-(dimethylamino)ethyl methacrylate) block copolymer as the gene carrier system: physicochemical properties of micelles relevant to gene transfection efficiency. *Biomacromolecules 5*, 2128−2136.

(20) Pierschbacher, M. D., and Ruoslahti, E. (1984) Cell attachment activity of fibronectin can be duplicated by small synthetic fragments of the molecule. *Nature 309*, 30−33.

(21) Pierschbacher, M. D., and Ruoslahti, E. (1984) Variants of the cell recognition site of fibronectin that retain attachment-promoting activity. *Proc. Natl. Acad. Sci. U.S.A. 81*, 5985−5988.

(22) Dechantsreiter, M. A., Planker, E., Mathä, B., Lohof, E., Hölzemann, G., Jonczyk, A., Goodman, S. L., and Kessler, H. (1999) *N*-Methylated cyclic RGD peptides as highly active and selective $\alpha_v\beta_3$ integrin antagonists. *J. Med. Chem. 42*, 3033−3040.

(23) Allen, T. M. (2002) Ligand-targeted therapeutics in anticancer therapy. *Nat. Rev. 2*, 750−763.

(24) Kim, W. J., Yockman, J. W., Lee, M., Jeong, J. H., Kim, Y.-H., and Kim, S. W. (2005) Soluble *Flt-1* gene delivery using PEI-*g*-PEG-RGD conjugate for anti-angiogenesis. *J. Controlled Release 106*, 224−234.

(25) Kim, W. J., Yockman, J. W., Jeong, J. H., Christensen, L. V., Lee, M., Kim, Y.-H., and Kim, S. W. (2006) Anti-angiogenic inhibition of tumor growth by systemic delivery of PEI-*g*-PEG-RGD/pCMV-sFlt-1 complexes in tumor-bearing mice. *J. Controlled Release 114*, 381−388.

(26) Marinelli, L., Gottschalk, K.-E., Meyer, A., Novellino, E., and Kessler, H. (2004) Human integrin $\alpha_v\beta_5$: homology modeling and ligand binding. *J. Med. Chem. 47*, 4166−4177.

(27) Bretscher, M. S. (1996) Moving membrane up to the front of migrating cells. *Cell 85*, 465−467.

(28) Marnie, R., Simon, B., Alison, W., Peter, S., and Jim, N. (2001) PDGF-regulated rab4-dependent recycling of $\alpha_v\beta_3$ integrin from early endosomes is necessary for cell adhesion and spreading. *Curr. Biol. 11*, 1392−1402.

(29) Suh, J., Wirtz, D., and Hanes, J. (2003) Efficient active transport of gene nanocarriers to the cell nucleus. *Proc. Natl. Acad. Sci. U.S.A. 100*, 3878−3882.

(30) Kulkarni, R. P., Wu, D. D., Davis, M. E., and Fraser, S. E. (2005) Quantitating intracellular transport of polyplexes by spatio-temporal image correlation spectroscopy. *Proc. Natl. Acad. Sci. U.S.A. 102*, 7523−7528.

(31) Rejmna, J., Bragonzi, A., and Conese, M. (2005) Role of clathrin- and caveolae-mediated endocytosis in gene transfer mediated by lipo- and polyplexes. *Mol. Ther. 12*, 468−474.

(32) Gersdorff, K., Sanders, N. N., Vandenbroucke, R., Smedt, S. C., Wagner, E., and Ogris, M. (2006) The internalization route resulting in successful gene expression depends on both cell line and polyethylenimine polyplex type. *Mol. Ther. 14*, 745−753.

BC0700133

ELSEVIER

Available online at www.sciencedirect.com
ScienceDirect

Journal of Controlled Release 122 (2007) 252–260

journal of controlled release

www.elsevier.com/locate/jconrel

PEG-based block catiomers possessing DNA anchoring and endosomal escaping functions to form polyplex micelles with improved stability and high transfection efficacy

Kanjiro Miyata [a,d], Shigeto Fukushima [b], Nobuhiro Nishiyama [c,d], Yuichi Yamasaki [b,d], Kazunori Kataoka [b,c,d,*]

[a] Department of Bioengineering, School of Engineering, The University of Tokyo, 7-3-1 Hongo, Bunkyo-ku, Tokyo 113-8656, Japan
[b] Department of Materials Engineering, School of Engineering, The University of Tokyo, 7-3-1 Hongo, Bunkyo-ku, Tokyo 113-8656, Japan
[c] Center for Disease Biology and Integrative Medicine, School of Medicine, The University of Tokyo, 7-3-1 Hongo, Bunkyo-ku, Tokyo 113-0033, Japan
[d] Center for NanoBio Integration, The University of Tokyo, 7-3-1 Hongo, Bunkyo-ku, Tokyo 113-8656, Japan

Received 26 May 2007; accepted 19 June 2007
Available online 27 June 2007

Abstract

For the development of polyplex systems showing a high transfection efficacy without a large excess of polycations, a lysine (Lys) unit as a DNA anchoring moiety was introduced into the amino acid sequence in poly(ethylene glycol)-*b*-cationic poly(*N*-substituted asparagine) with a flanking *N*-(2-aminoethyl)-2-aminoethyl group (PEG-*b*-Asp(DET)) resulting in PEG-*b*-P[Lys/Asp(DET)], in which the Asp(DET) unit acts as a buffering moiety inducing endosomal escape with minimal cytotoxicity. PEG-*b*-P[Lys/Asp(DET)]/DNA polyplexes exhibited a narrow size distribution of ~90 nm without secondary aggregates at the stoichiometric N/P 1, suggesting the formation of PEG-shielded polyplex micelles. The introduction of Lys units into the catiomer sequence facilitated cellular uptake and a 100-fold higher level of gene expression with PEG-*b*-P[Lys/Asp(DET)]/DNA polyplex micelles prepared even at a lowered N/P 2, possibly due to the enhanced association power of the anchoring Lys units.

Keywords: Gene delivery; PEG; Polyplex micelle; Block copolymer; Nonviral

1. Introduction

In recent years, enormous efforts have been devoted to the development of polycation-based gene delivery systems (polyplexes) due to their safety for clinical use, simplicity of preparation, and adaptability to large-scale production [1,2]. In particular, poly(ethylene glycol)-modified (PEGylated) polyplexes (polyplex micelles) formed through the electrostatic interaction between plasmid DNA (pDNA) and PEG-*b*-polycation copolymers (PEG-based block catiomers) are promising for *in vivo* gene therapy applications. The unique core-shell architecture of PEG-based block catiomers when combined with pDNA shows particle size data <100 nm under physiological conditions [3]. Indeed, polyplex micelles from PEG-*b*-poly(L-lysine) copolymers showed a high colloidal stability in biological media, excellent biocompatibility, and prolonged circulation periods in the blood stream [4–6]. However, further improvement in the transfection efficacy of these polyplex systems is needed for translation into the clinic.

Previous studies have revealed that a high transfection efficacy was obtained from polycations with a relatively low p*K*a value, such as polyethylenimine (PEI), which is explained by their buffering effect in endosomal compartments, as described by the proton sponge hypothesis [7,8]. In this regard, we have developed PEG-*b*-poly(*N*-substituted asparagine) copolymers having the *N*-(2-aminoethyl)-2-aminoethyl group

* Corresponding author. Department of Materials Engineering, School of Engineering, The University of Tokyo, 7-3-1 Hongo, Bunkyo-ku, Tokyo 113-8656, Japan. Fax: +81 3 5841 7139.
E-mail address: kataoka@bmw.t.u-tokyo.ac.jp (K. Kataoka).

0168-3659/$ - see front matter © 2007 Elsevier B.V. All rights reserved.
doi:10.1016/j.jconrel.2007.06.020

in the side chain (PEG-*b*-PAsp(DET)). Consequently, these polyplex micelles exhibited a remarkably high transfection activity possibly due to the high buffering capacity based on the distinctive two-step protonation behavior of the flanking ethylenediamine moiety [9]. Also, we found that PEG-*b*-PAsp (DET) copolymers showed minimal cytotoxicity, allowing the successful transfection to primary cells [9–12]. However, an excess of PEG-*b*-PAsp(DET) copolymers with high N/P ratios were required for successful polyplex transfection; consequently, we concluded that micelle solutions prepared under such conditions are likely to contain a mixed population of: (i) block catiomers firmly condensing DNA, (ii) block catiomers loosely associated with DNA, and (iii) free or non-DNA condensing block catiomers. Hence, *in vivo* use of such PEG-*b*-PAsp(DET) polyplex micelles, particularly for systemic administration, may be limited, because loosely associated block catiomers easily desorb from the polyplex micelles during blood circulation, leading to the decreased transfection efficacy at the target site. Therefore, the micelle systems showing efficient transfection at lower N/P ratios without such non-associated or loosely associated catiomers should be next developed for *in vivo* gene delivery.

The present study was devoted to improving the transfection efficacy of the PEG-*b*-PAsp(DET)-based polyplex micelles at N/P ratios near unity by enhancing their association power through the introduction of Lys residues into the amino acid sequence of the block catiomer. Note that Lys residues are expected to anchor the associated block catiomers to the polyplex micelles. In this way, a significantly improved efficacy of transfection was achieved with the polyplex micelles with a subtle excess of block catiomers even after preincubation in the medium containing serum. This result seems to be associated with the facilitated cellular internalization of the polyplex micelles with stably incorporated block catiomers showing a high buffering capacity for endosomal escape.

2. Materials and methods

2.1. Materials

α-Methoxy-ω-amino-poly(ethylene glycol) (Mw 12,000) and β-benzyl-L-aspartate *N*-carboxyanhydride (BLA-NCA) were obtained from Nippon Oil and Fats Co., Ltd. (Tokyo, Japan). ε-(Benzyloxycarbonyl)-L-lysine *N*-carboxyanhydride (Lys(Z)-NCA) was synthesized from ε-(benzyloxycarbonyl)-L-lysine (Wako Pure Chemical Industries, Ltd., Osaka, Japan) by the Fuchs–Farthing method using bis(trichloromethyl) carbonate (triphosgene) (Tokyo Kasei Kogyo Co., Ltd., Tokyo, Japan) [13]. Diethylenetriamine (DET), *N,N*-dimethylformamide (DMF), dichloromethane, benzene, and trifluoroacetic acid were purchased from Wako Pure Chemical Industries, Ltd. Hydrogen bromide (HBr) (30% in acetic acid) was purchased from Tokyo Kasei Kogyo Co., Ltd. Branched polyethylenimine (25 kDa) (BPEI) was purchased from Sigma-Aldrich Co. (St. Louis, MO). The pDNA coding for *luciferase* with a CAG promoter (RIKEN, Japan) was amplified in competent DH5α *E. coli* and purified with a QIAGEN HiSpeed Plasmid MaxiKit (Germantown, MD). Luciferase Assay System Kit was purchased from Promega (Madison WI); Label IT Fluorescein Labeling Kit from Mirus Co. (Milwaukee, WI); and Micro BCA™ Protein Assay Reagent Kit from Pierce Co., Inc. (Rockford, IL).

2.2. Synthesis of PEG-b-P[Lys/Asp(DET)]

Block copolymers of PEG and L-lysine(Z)/β-benzyl-L-aspartate copolymer (P[Lys(Z)/BLA]), further referenced as PEG-*b*-P[Lys(Z)/BLA], were synthesized by ring-opening polymerization of a mixture of Lys(Z)-NCA and BLA-NCA initiated by the terminal primary amino group of α-methoxy-ω-amino-PEG (Scheme 1). The typical synthetic procedure is described as follows for the PEG-*b*-P[Lys(Z)/BLA] with 47 units of Lys(Z) and 52 units of BLA. Lys(Z)-NCA (1.29 g) and BLA-NCA (1.25 g) were dissolved in a mixture of DMF and dichloromethane (6.8 mL and 31.7 mL, respectively). This NCA solution was added to the PEG (1.0 g) in dichloromethane (15 mL) in a stream of dry argon and stirred at 35 °C for 48 h for copolymerization. The polymer in the reaction medium was precipitated in a mixture of hexane and ethyl acetate (600 mL and 400 mL, respectively), and purified by filtration. The acetylation of the *N*-terminal amino group of the obtained polymer (1.5 g) was subsequently performed at 35 °C for 1 h using acetic anhydride (500 μL) in a dichloromethane solution (22 mL). The polymer solution was precipitated into a mixture of hexane and ethyl acetate (300 mL and 200 mL, respectively), purified by filtration, and lyophilized from a benzene solution. The resulting copolymers had molecular weight distributions (Mw/Mn) of 1.1 to 1.3 as determined by GPC (data not shown). The degree of polymerization (DP) of the P[Lys(Z)/BLA] segment in the PEG-*b*-P[Lys(Z)/BLA] was determined from the peak intensity ratio of the methylene protons of PEG (OCH_2-CH_2, δ=3.5 ppm) to the aryl protons of the benzyl groups in the

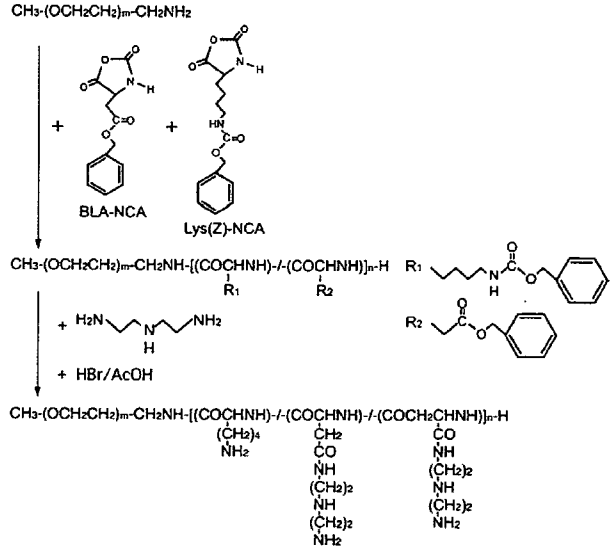

Scheme 1. Synthetic procedure of PEG-*b*-P[Lys/Asp(DET)].

Lys(Z) and BLA units (C_6H_6, δ=7.2–7.3 ppm) in the ^{1}H NMR spectra taken in dimethylsulfoxide at 80 °C. The compositions of the P[Lys(Z)/BLA] segments were determined from the peak intensity ratio of the protons of the β to δ methylene groups ($CH_2CH_2CH_2$, δ=1.2–2.0 ppm) in the side chain of the Lys(Z) units to the protons of the benzyl groups in the Lys(Z) and BLA units in the ^{1}H NMR spectra under the same conditions.

The PEG-*b*-P[Lys(Z)/BLA] copolymers (300 mg) were dissolved in DMF (6 mL), after which DET (2.5 mL; 50 eq to the benzyl group of PBLA) was added to the polymer solution, and stirred for 24 h at 40 °C under a dry argon atmosphere. After 24 h, the mixture was dropped into diethylether (120 mL) with stirring, and then the white precipitate was filtered and re-dissolved in trifluoroacetic acid (4 mL). To deprotect the Z group, HBr (30% in acetic acid) was then added and stirred for 1 h, after which the solution was dropped into diethylether (100 mL) with stirring, and the resulting precipitate was purified by filtered and dried *in vacuo*. The crude product was dissolved in distilled water, dialyzed against 0.01 N HCl and distilled water, and lyophilized to obtain the final product, PEG-*b*-P[Lys/Asp(DET)] as the hydrochloride salt form. The PEG-*b*-P[Lys/Asp(DET)] copolymers with varying ratios of Lys units to Asp (DET) units were obtained by changing the initial feeding ratio of Lys(Z)-NCA to BLA-NCA upon polymerization. The introduction of a DET moiety was confirmed from the peak intensity ratio of the methylene protons of PEG (OCH_2CH_2, δ=3.5 ppm) to the methylene protons of the introduced DET moieties ($CH_2CH_2NHCH_2CH_2$, δ=2.6–3.6 ppm) in the ^{1}H NMR spectra taken in D_2O at 25 °C.

2.3. Preparation of polyplex micelles from PEG-b-P[Lys/Asp (DET)]

The synthesized PEG-*b*-P[Lys/Asp(DET)] copolymer was dissolved in 10 mM Tris–HCl (pH 7.4) buffer at 5 mg/mL. This polymer solution was then mixed with pDNA in 10 mM Tris–HCl (pH 7.4) (50 μg/mL) at varying N/P ratios (residual molar ratio of amino groups in Lys and Asp(DET) units to pDNA phosphate groups), followed by a 24 h incubation at ambient temperature. The final concentration of pDNA in all the samples was adjusted to 33 μg/mL. The complexation of pDNA with the polycations was confirmed by agarose gel retardation analysis and ethidium bromide (EtBr) dye exclusion assay. In the gel retardation analysis, each sample was prepared by the dilution of the micelle solutions to the concentration of 8.3 μg pDNA/mL. 20 μL of each sample (166 ng pDNA) with a loading buffer was then electrophoresed at 100 V for 1 h on a 0.9 wt% agarose gel in 3.3 mM Tris–acetic acid buffer containing 1.7 mM sodium acetate. The migrated pDNA was visualized by soaking the gel in distilled water containing EtBr (0.5 μg/mL). In the EtBr dye exclusion assay, each sample (33 μg pDNA/mL) with varying N/P ratios was adjusted to 10 μg pDNA/mL with 2.5 μg EtBr/mL and 150 mM NaCl by adding 10 mM Tris–HCl (pH 7.4) buffer containing EtBr and NaCl. The solutions were incubated at ambient temperature overnight. The fluorescence intensity of the samples excited at 510 nm was measured at 590 nm and a temperature of 25 °C using a spectrofluorometer (Jasco, FP-777). The relative fluorescence intensity was calculated as follows:

$$F_r = (F_{sample} - F_0)/(F_{100} - F_0)$$

where F_{sample} is the fluorescence intensity of the micelle samples, F_{100} is the free pDNA, and F_0 is the background without pDNA.

2.4. Zeta-potential and dynamic light scattering (DLS) measurements

The zeta-potential of the polyplex micelles was determined from the laser-Doppler electrophoresis using the Zetasizer nanoseries (Malvern Instruments Ltd., UK) at a detection angle of 173° and a temperature of 25 °C. Each sample was prepared by simply mixing the polymer solutions with the pDNA solution at varying N^+/P ratios (33 μg pDNA/mL). The N^+/P ratio was defined as the residual molar ratio of protonated amino groups in PEG-*b*-P[Lys/Asp(DET)] to phosphate groups in DNA. The fraction of protonated amino groups in P[Lys/Asp(DET)] segment was calculated assuming that 100% and 50% of the amino groups in the Lys and Asp(DET) units, respectively, were protonated at pH 7.4 and a temperature of 25 °C based on the potentiometric titration results [9]. The samples were adjusted to 14 μg pDNA/mL by adding 10 mM Tris–HCl (pH 7.4) buffer, and then, injected into folded capillary cells (Malvern Instruments, Ltd.), followed by the measurement. From the obtained electrophoretic mobility, the zeta-potentials of each micelle were calculated by the Smoluchowski equation: $\zeta = 4\pi\eta\upsilon/e$ in which η is the viscosity of the solvent, υ is the electrophoretic mobility, and e is the dielectric constant of the solvent. The results are represented as the average of three experiments.

The sizes of each polyplex micelle were also measured by the DLS using the same apparatus. Micelle samples were prepared by mixing each polymer solution with pDNA solution at varying N^+/P ratios (33 μg pDNA/mL). After an overnight incubation at ambient temperature, the samples were adjusted to 14 μg pDNA/mL by adding 10 mM Tris–HCl (pH 7.4) buffer, and then injected into low volume glass cuvettes, ZEN2112 (Malvern Instruments, Ltd.), followed by the measurement. The data obtained from the rate of decay in the photon correlation function were analyzed by the cumulant method, and the corresponding hydrodynamic diameter of micelles was then calculated by the Stokes–Einstein equation [14].

2.5. Stability of polyplex micelles against counter polyanion exchange reaction

The stability of the polyplex micelle was estimated from the release of pDNA from the micelle caused by the exchange reaction with poly(aspartic acid) (PAsp, DP 66) as a polyanion. Ten mM Tris–HCl buffer (pH 7.4) solutions with varying concentrations of PAsp were added to the micelle solution with the pDNA concentration of 33 μg/mL. After overnight incubation at ambient temperature, each sample solution containing 167 ng of pDNA was electrophoresed through a 0.9 wt% agarose gel with

a running buffer of (3.3 mM Tris–acetic acid (pH 7.4)+1.7 mM sodium acetate+1 mM EDTA2Na). The pDNAs in the gel were visualized by soaking the gel into distilled water containing EtBr (0.5 mg/L).

2.6. Radiolabeling of pDNA for the cellular uptake study of polyplex micelles

pDNA was radioactively labeled with ^{32}P-dCTP using the Nick Translation System (Invitrogen, San Diego, CA). Unincorporated nucleotides were removed using High Pure PCR Product Purification Kit (Roche Laboratories, Nutley, NJ). After the purification, the 2 μg of labeled pDNA was mixed with 400 μg of non-labeled pDNA. The polyplex micelle samples were prepared by mixing the radioactive pDNA solution with each polymer solution (33 μg pDNA/mL). For cellular uptake experiments, Hela cells were seeded on 24-well cultured plates 24 h before the experiments in Dulbecco's modified Eagle medium (DMEM) containing 10% fetal bovine serum (FBS). The cells were incubated with 30 μL of the radioactive micelle solution (1 μg pDNA/well) in 400 μL of DMEM containing 10% FBS. After 24 h incubation, the cells were washed three times with Dulbecco's PBS and lysed with 400 μL of the cell culture Promega lysis buffer. The lysates were mixed with 5 mL of scintillation cocktail, Ultima Gold (PerkinElmer, MA), and then, the radioactivity of the lysate solution was measured by a scintillation counter. The results are presented as a mean and standard error of mean obtained from four samples.

2.7. In vitro transfection

Hela cells were seeded on 24-well culture plates and incubated overnight in 400 μL of DMEM containing 10% FBS. The medium was changed to 400 μL of fresh DMEM containing 10% FBS, and then 30 μL of each micelle solution was applied to each well (1 μg of pDNA/well). In the estimation of the effect of serum incubation on the transfection capacity of the micelle samples, the micelle solutions were preincubated with DMEM containing 10% FBS for 4 h and then added to the wells. After 24 h incubation, the medium was changed to 400 μL of fresh DMEM without micelle samples, followed by an additional 24 h incubation. The cells were washed with 400 μL of Dulbecco's PBS, and lysed by 100 μL of the cell culture Promega lysis buffer. The luciferase activity of the lysates was evaluated from the photoluminescence intensity using Mithras LB 940 (Berthold Technologies). The obtained luciferase activity was normalized with the amount of proteins in the lysates determined by the Micro BCA™ Protein Assay Reagent Kit (Pierce).

Table 1
A series of synthesized block catiomers

Code	Feeding unit radio (Lys: Asp)	DP of poly (amino acid)	Unit number of Lys in poly(amino acid)	% of Lys units
L0/101	0:120	101	0	0
L24/102	25:90	102	24	24
L47/99	50:60	99	47	47
L70/98	75:30	98	70	71
L109/109	120:0	109	109	100

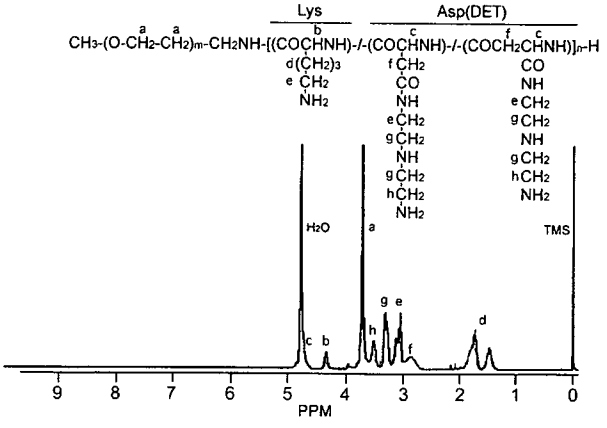

Fig. 1. ^{1}H-NMR spectrum of the PEG-*b*-P[Lys/Asp(DET)] (L47/99) (D_2O; 25 °C; concentration, 10 mg/mL).

2.8. Tolerability of polyplex micelles in serum-containing medium

The tolerability of polyplex micelles in serum-containing medium was estimated from the change in the fluorescence intensity of the fluorescein-labeled pDNA (F-pDNA) contained in the micelles. A pDNA was labeled using a Label IT Fluorescein Labeling Kit. This system promotes the covalent attachment of specific fluorescent molecules to guanine residues in nucleic acids. Each polyplex micelle sample was prepared by simply adding the polymer solution to the F-pDNA solution. After an overnight incubation at ambient temperature under dark conditions, the micelle solutions were mixed with 9 times volume of FBS solution, and then incubated at 37 °C for 4 h. The fluorescence emission of each sample excited at 492 nm was measured at 520 nm and a temperature of 37 °C using a spectrofluorometer (Jasco, FP-777). The obtained fluorescence intensities were expressed as the relative value to the fluorescence intensity of naked F-pDNA.

3. Results and discussion

3.1. Synthesis of PEG-b-P[Lys/Asp(DET)]

Block copolymers of PEG and P[Lys(Z)/BLA] (PEG-*b*-P[Lys(Z)/BLA]) were prepared by the ring-opening copolymerization of Lys(Z)- and BLA-NCAs as shown in Scheme 1. The poly(amino acid) segments with similar DP and varying Lys(Z)/BLA unit ratios were synthesized by changing the feeding ratio of Lys(Z)-NCA to BLA-NCA in the reaction mixture. The DPs and the unit ratios of Lys(Z)/BLA in the obtained copolymers were calculated from the peak intensity ratio in the ^{1}H NMR spectra (data not shown). As summarized in Table 1, five types of copolymers were prepared. The DP of the poly(amino acid) segments in a series of copolymers was confirmed to be approximately 100, regardless of the composition. These copolymers were then subjected to aminolysis reaction with DET, followed

by deprotection of the Z groups. The ^{1}H NMR spectra of the obtained catiomers, as typically seen in Fig. 1, reveal the quantitative aminolysis of BLA units as well as the complete deprotection of Lys(Z) units in the poly(amino acid) segment, because the methylene protons in the DET moiety and the β-methylene protons in the asparagine unit had a 4:1 peak intensity ratio and the peaks of the Z group disappeared in the ^{1}H NMR spectrum. These catiomers were abbreviated as L*x*/*y*, where *x* and *y* represent the unit number of Lys and the total DP of the poly(amino acid) segment, respectively.

3.2. Formation of polyplex micelles from PEG-b-P[Lys/Asp (DET)] catiomers

The polyplex micelles were prepared by simply mixing each catiomer solution with pDNA solution at varying N/P ratios. The complex formation of pDNA was confirmed by the agarose gel electrophoresis of each sample. With an increase in the N/P ratio, the amount of migrating free pDNA decreased, indicating the complex formation of pDNA with the PEG-*b*-P[Lys/Asp (DET)] catiomers (Supplementary Fig. 1). The critical N/P ratio where the migration of pDNA was completely retarded differed depending on the composition of the catiomers; i.e., the micelle of the block catiomers with a lower ratio of Lys units required the higher N/P ratio for the complete retardation of pDNA. To quantitatively evaluate the relationship between the N/P ratio and the condensation behavior of pDNA, the EtBr dye exclusion assay by fluorometry was completed. Fig. 2 (a) shows that the fluorescence intensity of EtBr decreased with an increase in the N/P ratio, and leveled off at a critical N/P ratio for each micelle system. These fluorescence data were then replotted against N^+/P ratio, the molar ratio of protonated amino groups at pH 7.4 in the block catiomers to phosphate groups in pDNA, as seen in Fig. 2 (b). Note that the ratios of the protonated amino groups in the block catiomer were calculated as 100% for Lys units and 50% for Asp(DET) units at pH 7.4, respectively, from the potentiometric titration results of PEG-*b*-PLys and PEG-*b*-PAsp(DET) block catiomers [9,15]. Interestingly, Fig. 2 (b) reveals that the fluorescence intensity of all the micelles leveled off at the N^+/P ratio of approximately 1 regardless of the composition of the catiomers, indicating that the condensation behavior of pDNA might be closely correlated with the ratio of charged groups (N^+/P). Also, this result strongly suggests that the PAsp(DET) segment in the micelles is likely to maintain the same protonation degree ($\alpha = 0.5$ at pH 7.4) as that in the free catiomer without the facilitated protonation by the complexation. As previously reported [9], this limited protonation for the proton sponge potential of the Asp(DET) units in the micelles is assumed to contribute to endosomal escape of PEG-*b*-P[Lys/Asp(DET)] polyplex micelles.

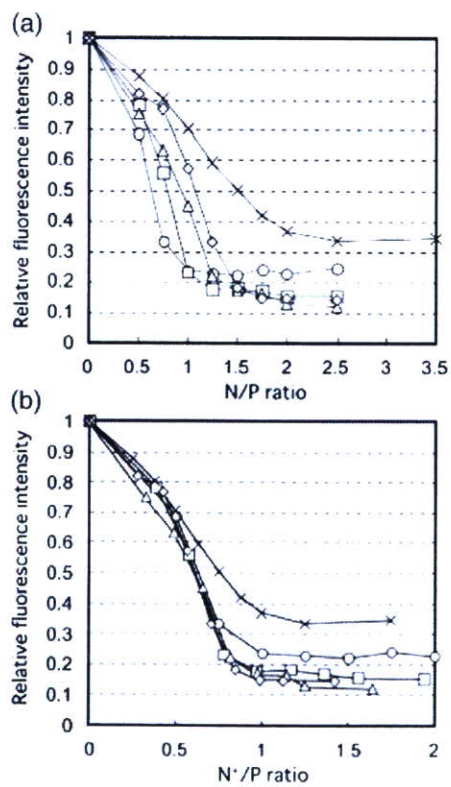

Fig. 2. EtBr dye exclusion assay on a series of polyplex micelles. Micelles included are: ×: L0/101; ◇: L24/102; △: L47/99; □: L70/98; ○: L109/109. (a) Relative fluorescence intensity vs. N/P ratio. (b) Relative fluorescence intensity vs. N^+/P ratio.

Fig. 3 (a) and (b) show the results obtained from DLS and zeta-potential measurements. The cumulant diameters of the polyplex micelles from the PEG-*b*-P[Lys/Asp(DET)]s were determined to be 70–100 nm throughout the range of the examined $N^+/P > 1$. As seen in the Fig. 3 (b) inset, the zeta-potentials of each polyplex micelle appear nearly neutral at an N^+/P 1, indicating the formation of the charge stoichiometric micelle from pDNA and the block catiomers. It should be emphasized that the polyplex micelles from PEG-*b*-P[Lys/Asp(DET)] had a narrowly distributed size of approximately 90 nm without secondary aggregates even at the charge neutralized condition (N^+/P 1) as previously demonstrated for those from PEG-*b*-PLys and PEG-*b*-PAsp(DET) catiomers [9,16]. It should also be noted that all polyplex micelles from the block catiomers had a much lower absolute value in zeta-potentials than polyplexes prepared from PAsp(DET) homopolymer (DP 98) (Fig. 3 (b)), possibly due to the shielding effect of the PEG layer surrounding the polyplex core. Nevertheless, there was a slight increase in the zeta-potentials of the polyplex micelles from neutral to positive values in the region of $N^+/P > 1$. This zeta-potential increase is likely to be ascribed to the loose association of excess catiomers with the polyplex micelles as previously reported for the PEG-poly(2-dimethylamino)ethyl methacrylate) catiomer/pDNA micelle [17]. Interestingly, the tendency of such increasing zeta-potentials with N^+/P ratios varied according to the composition of the block catiomers. The zeta-potential value of the polyplex micelles from PEG-*b*-PLys leveled off at an N^+/P 4 (+10 mV), while that from PEG-*b*-PAsp(DET) seemed to reach a plateau at a higher N^+/P 16 (+10 mV), suggesting that the association profile of the block catiomers with the polyplex micelles varied between PEG-*b*-PLys and PEG-*b*-PAsp(DET) micelles at N^+/P ratios ranging from 1 to 16. Presumably, PEG-*b*-PLys may reach the saturated association with pDNA at the lower

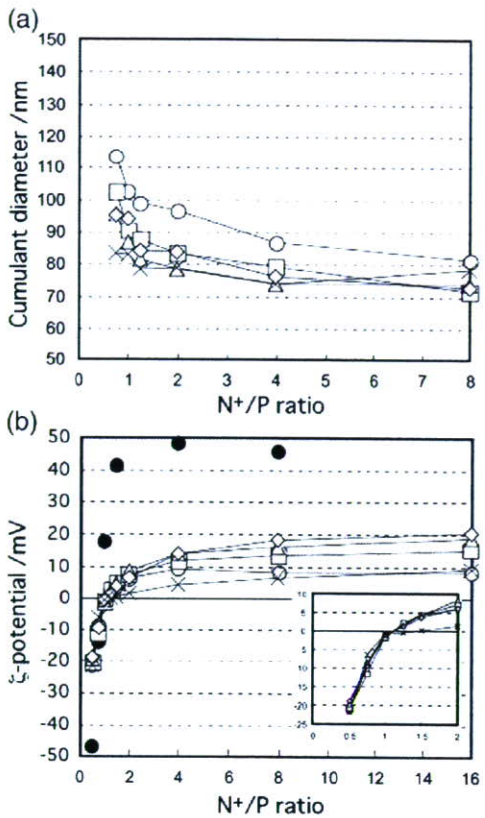

Fig. 3. (a) Size and (b) ζ-potential of a series of polyplex micelles and a PAsp (DET) polyplex. ×: L0/101 micelle, ◇: L24/102 micelle, △: L47/99 micelle, □: L70/98 micelle, ○: L109/109 micelle, ●: PAsp(DET) (DP 98) polyplex.

concentration (lower N^+/P) than PEG-*b*-PAsp(DET) due to the effective anchoring effect of the Lys units. Although PEG-*b*-P[Lys/Asp(DET)] micelles displayed the similar profiles of the zeta-potential to PEG-*b*-PLys micelles at lower N^+/P ratios, the micelles showed further increase in the surface charge in the range of $N^+/P > 4$ without leveling off. This result suggests that the association of PEG-*b*-P[Lys/Asp(DET)] with pDNA may not be saturated even in the range of $N^+/P > 4$, despite introduction of Lys units as a DNA anchoring moiety. This phenomenon may be ascribed to the unique structure of PEG-*b*-P[Lys/Asp(DET)] possessing two types of cationic units with different pDNA affinity. The presence of the Lys units in the block catiomer is likely to facilitate the binding of Asp (DET) units to pDNA, promoting the block catiomer association to the polyplex micelles at N^+/P 2 or lower; however, at high concentrations of the block catiomers (high N^+/P), Lys units may preferentially bind to the polyplex micelles to replace the Asp (DET) units, resulting in the continuous binding of the block catiomers until the Lys units saturate the available binding sites.

3.3. Stability of polyplex micelles

The result of the zeta-potential measurement suggested that the affinity of PAsp(DET) to pDNA seems to be enhanced by the incorporation of Lys units. The complexing stability of the polyplex micelles prepared from PEG-*b*-P[Lys/Asp(DET)] was evaluated directly from the standpoint of the counter polyion exchange reaction. The solutions with varying concentrations of PAsp were added to the solution of the PEG-*b*-PAsp(DET) micelle (N^+/P 2) in different A/P ratios (the molar ratio of carboxyl groups of PAsp to phosphate groups of pDNA). Consequently, the pDNA was released from the PEG-*b*-PAsp (DET) micelles at $A/P > 3$ due to the counter polyanion exchange of pDNA by PAsp (Fig. 4 (a)). In contrast, the improved stability of the polyplex micelles from PEG-*b*-P[Lys/Asp(DET)] was

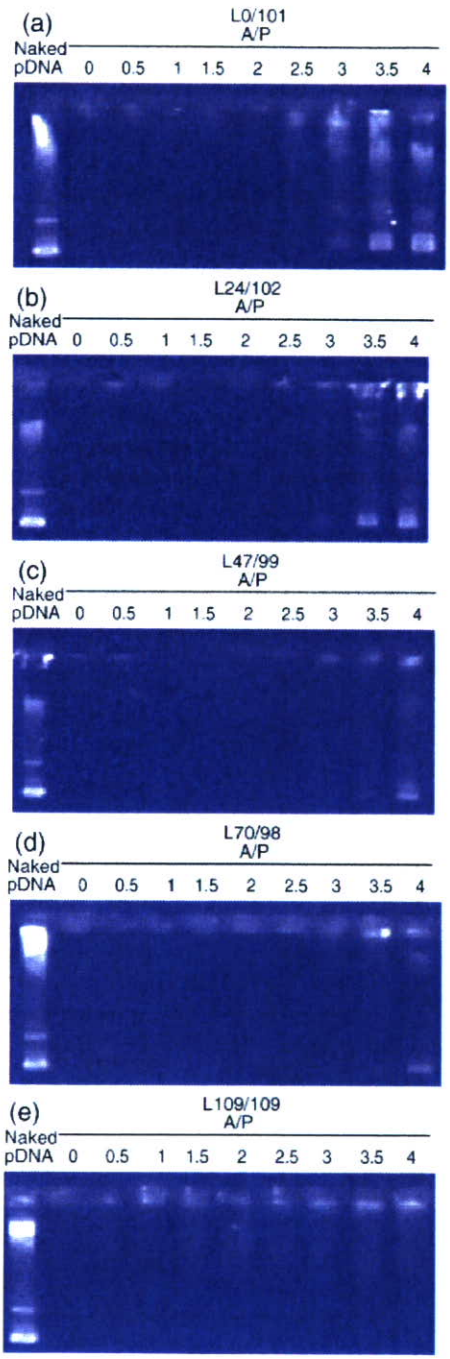

Fig. 4. Electrophoretic evaluation of polyplex micelle (N^+/P 2) tolerability against an exchange reaction with polyaspartic acid (DP 66). Note: A/P stands for the molar ratio of carboxyl groups in polyaspartic acid to phosphate groups in pDNA. Micelle samples prepared at N^+/P 2 were mixed with polyaspartic acid solution and electrophoresed after overnight incubation.

confirmed as shown in Fig. 4 (b)–(d): higher A/P ratios were required for the pDNA release with the increment in the percentage of Lys units in the amino acid sequence of the PEG-*b*-P[Lys/Asp(DET)]. In the case of the micelles from PEG-*b*-PLys, the pDNA release was not observed in the range of the examined A/P ratios (0–4) (Fig. 4 (e)). The similar tendency was also confirmed for the micelles prepared at N^+/P 4 (Supplementary Fig. 2). These results support our hypothesis that a Lys unit has a higher association power with pDNA than the Asp(DET) unit, and consequently, the PEG-*b*-P[Lys/Asp(DET)] micelles acquired the tolerability against the dissociation by polyanions through the anchoring effect of Lys units in the block catiomer.

3.4. Transfection with polyplex micelles from PEG-b-P[Lys/Asp(DET)]

Preliminary experiments on the cellular uptake of complexed pDNA revealed that the pDNA incorporated into PEG-*b*-PAsp (DET) at $N^+/P < 4$ was marginally internalized by cultured cells as is the case with naked pDNA (Supplementary Fig. 3). We speculate that this may contribute to the significantly lower transfection ability of PEG-*b*-PAsp(DET) micelles prepared at low N^+/P ratios. Herein, we hypothesize that the complexing stability promoted by the Lys anchors may facilitate the cellular uptake of polyplex micelles prepared even at low N^+/P ratios. To confirm this hypothesis, we completed a cellular uptake study using ^{32}P-radiolabeled pDNA. Fig. 5 reveals that the cellular uptake of pDNA complexed with block catiomers at an N^+/P ratio of 2 increased by the introduction of the Lys unit into the amino acid sequence. Especially, the polyplex micelles from the PEG-*b*-P[Lys/Asp(DET)] with the percentage of Lys units >47 exhibited more than a 10-fold uptake of pDNA compared to PEG-*b*-PAsp (DET). This result strongly suggests that the increased association power of the polyplex micelles may contribute to their facilitated cellular uptake without a large excess of block catiomers, i.e., at low N^+/P ratios. Interestingly, the cellular uptake of radioactive pDNA was maximized at the L70/98, even through its stability was deemed comparable to that of PEG-*b*-PLys (L109/109), as evidenced from the counter polyanion exchange reaction (Fig. 4

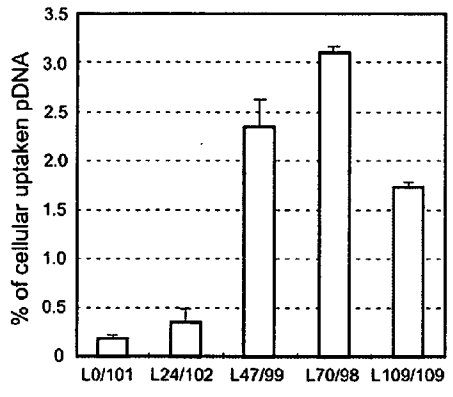

Fig. 5. The uptake of pDNA complexed with block catiomers at N^+/P 2 into Hela cells. ^{32}P-labeled pDNA micelles were incubated with the cells in DMEM containing 10% FBS at 37 °C for 24 h. The amount of internalized pDNA is represented as a percentage for the dosed pDNA (1 μg/well).

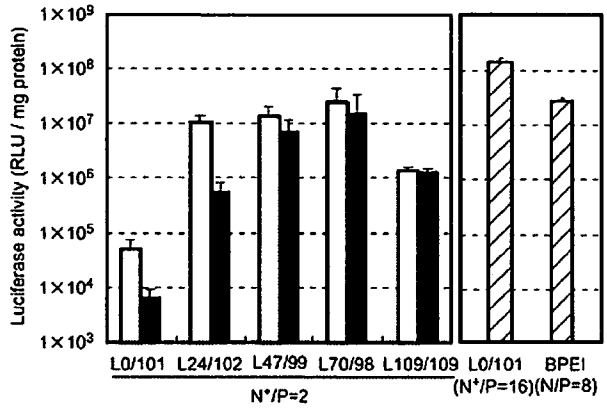

Fig. 6. *In vitro* transfection efficacy of polyplex micelles (N^+/P 2) against Hela cells. Open bars: Transfection efficacy without serum-preincubation. Closed bars: Transfection efficacy after 4 h incubation in the DMEM containing 10% FBS. Hatched bars: Transfection efficacy of the control; L0/101 micelles (N^+/P 16) and BPEI (25 kDa) polyplexes (N/P 8).

(d) and (e)). These data indicate that the increased cellular uptake of PEG-*b*-P[Lys/Asp(DET)] micelles compared to PEG-*b*-PLys micelles was not simply correlated to the enhanced stability. In this regard, a slightly positive zeta-potential of PEG-*b*-P[Lys/Asp (DET)] micelles compared to PEG-*b*-PAsp(DET) and PEG-*b*-PLys micelles is noteworthy, suggesting the surface charge may indeed affect the cellular uptake of the micelles with varying stabilities.

The effect of the introduction of the Lys unit as an anchoring moiety on the transfection ability of the polyplex micelles was then evaluated from the expression of a luciferase gene in the transfected cells. Although the PEG-*b*-PAsp(DET) micelles prepared at the high N^+/P 16 (ca. N/P 32) showed appreciably high transfection efficacy, which was one order of magnitude higher than that of BPEI polyplexes (25 kDa, N/P 8), reduction in the N^+/P ratio resulted in a sharp decline of the transfection ability of the PEG-*b*-PAsp(DET) micelles probably due to the lowered cellular uptake (Fig. 6). In contrast, the transfection efficacy could be maintained to be a high value even in the range of lowered N^+/P ratios by introducing Lys units into the block catiomer (Supplementary Fig. 4). Eventually, the PEG-*b*-P[Lys/Asp(DET)] micelles revealed an appreciably improved transfection efficacy at N^+/P 2 compared to the polyplex micelles of PEG-*b*-PLys and PEG-*b*-PAsp(DET) (Fig. 6, open bars). These results suggest that PEG-*b*-P[Lys/Asp(DET)] micelles may provide high stability and promote endosomal escape, presumably due to the synergistic effect of Lys and Asp(DET) units. The improved stability through the anchoring effect of Lys units was also confirmed from the transfection results after the preincubation of micelles in the serum-containing medium (Fig. 6, closed bars). The micelles from PEG-*b*-P[Lys/Asp(DET)], with the higher percentage of Lys units (L47/99 and L70/98), maintained the initial transfection capacity even after the serum-preincubation, whereas transfection efficacies of PEG-*b*-PAsp(DET) and L24/102 micelles, with a low percentage of Lys residues, were significantly impaired by serum-preincubation. These results strongly suggest that the associated block catiomers in the micelles from L47/99, L70/98, and L109/109 might be tolerable